Mask-Constrained Synthesis of Domino-Like Tiled Phased Arrays

Luca Tosi and Arianna Benoni*

Abstract—In this work, the mask-constrained synthesis of domino-tiled phased arrays is addressed. By exploiting tiling theorems and theory, optimal and sub-optimal methods for the synthesis of domino arrangements and the corresponding excitations that minimize the deviation of the radiation pattern from a user-defined power mask are presented. A set of numerical examples, carried out with full-wave simulators and concerned with different aperture sizes and various mask shapes, is reported to assess the effectiveness, limitations, and ranges of computationally-admissible applicability of the proposed methods.

1. INTRODUCTION

Modern radar/sensing and 5G communication applications require antennas with beam-shaping and steering capabilities, guaranteeing low costs and low weight architectures. Accordingly in the last years, methodologies for the synthesis of unconventional phased array architectures [1] (e.g., sparse [2], thinned [3, 4], and clustered arrays [1]), reflectarray-based systems [5, 6] and corporate feed-based technologies like the substrate integrated waveguide array [7] have been widely studied. Among these, clustered arrays are gaining a lot of attention thanks to their modular structures and reduce the complexity of the feeding network [1]. Generally speaking, *array clustering* consists in grouping two or more elements to be fed by a single transmission/reception module (TRM), while fulfilling the design objectives of the array synthesis at hand (e.g., the side lobe level minimization, the fitting of a radiation pattern with a user-defined mask, etc.) The reduction of the control points/TRMs with respect to a fully-populated (i.e., a TRM for each array element) architecture has a non-negligible impact on the radiation performance of the arising modular system since the radiated pattern unavoidably deviates from the ideal one. Moreover, high quantization lobes appear in case of a *periodic clustering* because of the regular quantization of the aperture distribution. To yield the optimal trade-off between TRMs reduction and closeness to the ideal radiation performance also avoiding undesired lobes, irregular/a-periodic phased array clustering for both linear [8–11] and planar [12–16] geometries has been widely studied in the recent years. Effective strategies for the computation of the sub-array weights (i.e., the complex excitations of the shared TRM modules), such as the analytic excitations matching (EM) technique [8, 9, 15] and hybrid methods combining evolutionary algorithms with convex programming (CP) solvers [10], have been proposed. As for the optimization of the clustering layout, efficient local-search techniques that guarantee a fast convergence to effective, even though sub-optimal, unconstrained clustered solutions (*unconstrained clustering*), for instance, the Contiguous Partition Method (CPM) [9, 11] and the Weighted K-means Clustering Method ($WKCM$) [15], have been developed. However, to the best of the authors' knowledge no one of these methods allows one to *a-priori* set the size/shape of the array partitions, while such a solution (the so-called *constrained clustering*) would enable a further cost saving. Indeed, besides the minimization of the number of TRMs, having

simpler sub-arrays with similar shapes would facilitate the modular assembling of the radiating system as well as the implementation of few production lines, one for each type of elementary building block [17]. Moreover, the modularity is advantageous in phased array antenna manufacturing since it enables the implementation of light and low profile structures [17], an easy maintenance, and integrated cooling systems [18]. The constrained clustering is also referred to as array tiling [14], *tiles* (i.e., physically contiguous clusters of elements) with the same shape (i.e., *single-shape tiling* [16, 19–25]) or a limited number of shapes (i.e., *multi-shape tiling* [12–14, 26, 27]), being used to cover the whole antenna aperture without overlapping and any gaps or leaving the minimum one. As a matter of fact, while a suitable shape/dimension of the antenna aperture is necessary to comply with the design constraints, modern radar/communication applications usually require high directive beams, which are admissible only when assuring the entire aperture overlay. In the mathematical literature, the tiling of a bounded area is known as *finite tiling problem*, and it is a non-trivial task [28–31], even the counting of the number of existing tilings for medium/large apertures is generally an almost computationally intractable/impossible task. However, there are mathematical theorems that allow one to assess the tilability of arbitrary rectangular regions [29] and to know the number of full-coverage tiling arrangements [32] in the case of *domino* tiles (i.e., 2-cells polyominos). By exploiting such a theoretical stuff, domino-based architectures have been studied in [20], and useful synthesis methods have been proposed. More specifically, exhaustive as well as *GA*-based methodologies have been proposed for minimizing the power pattern *SLL*, while ensuring the complete tessellation of the antenna aperture, by considering an efficient height-function [33] coding for the representation of the solution space and optimal tiling algorithms [34].

In this paper, a new class of tiling approaches is presented to properly address the mask-constrained array synthesis problem. Starting from a set of requirements on the array performances, which are set through a power mask, the proposed methods are aimed at finding the optimal tiling configuration affording a pattern that fits the mask or minimizes the deviation from it when the mask-matching at hand is not physically-admissible. More specifically, three synthesis approaches, namely the *ETM-CP*, *EM-ETM/CP*, and *EM-OTM/CP* methods, are formulated and their applications as well as feasibility are discussed when dealing with different array sizes and various mask requirements.
The outline of the paper is as follows. The mask constrained array tiling problem is formulated in Section 2 along with a detailed description of the proposed synthesis methods. Section 3 is devoted to the numerical validation of such techniques by considering different apertures and power masks shapes. Suitable guidelines and range of reliability/effectiveness of each approach are also suggested. The use of a full-wave solver for modelling real arrays is also considered to give a real assessment of the synthesis results. Some conclusions and final remarks are finally drawn (Section 4).

2. MATHEMATICAL FORMULATION

Let us consider a rectangular phased array [Fig. 1(a)] of $N_{tot} = M \times N$ elementary sources located in a lattice of square cells centered at the coordinates $(x_{m,n}, y_{m,n})$, $m = 1, \ldots, M$; $n = 1, \ldots, N$, and spaced by d_x and d_y along the x and y axes, respectively. The radiated power pattern $P(u, v)$ is given by

$$P(u, v) = \left| \sum_{m=1}^{M} \sum_{n=1}^{N} w_{m,n} EF_{m,n}(u, v) e^{jk(ux_{m,n} - vy_{m,n})} \right|^2 \tag{1}$$

where $k = \frac{2\pi}{\lambda}$ is the wavenumber; λ is the wavelength; $u \triangleq \sin\theta \cos\phi$ and $v \triangleq \sin\theta \sin\phi$ are the angular coordinates, while $w_{m,n}$ and $EF_{m,n}$ are the complex excitation and embedded element factor of the (m, n)-th array element, respectively. Dealing with a domino-tiling of the aperture, the array elements are vertically or horizontally grouped into Q rectangular sub-arrays of two elements each, namely a vertical σ_V or horizontal σ_H domino [Fig. 1(b)]. The output port of each q-th ($q = 1, \ldots, Q$) domino is then weighted by a complex coefficient w_q of amplitude α_q and phase β_q (i.e., $w_q = \alpha_q e^{j\beta_q}$). By mathematically describing a domino partition of the array aperture with the clustering vector $\underline{C} = \{c_{m,n} \in [1 \div Q]; m = 1, \ldots, M; n = 1, \ldots, N\}$, with its (m, n)-th integer entry being the membership of the (m, n)-th lattice element to the q-th tile, the corresponding radiated power pattern, $P(u, v)$, is obtained substituting in (1) the following excitations coefficients of the equivalent fully-
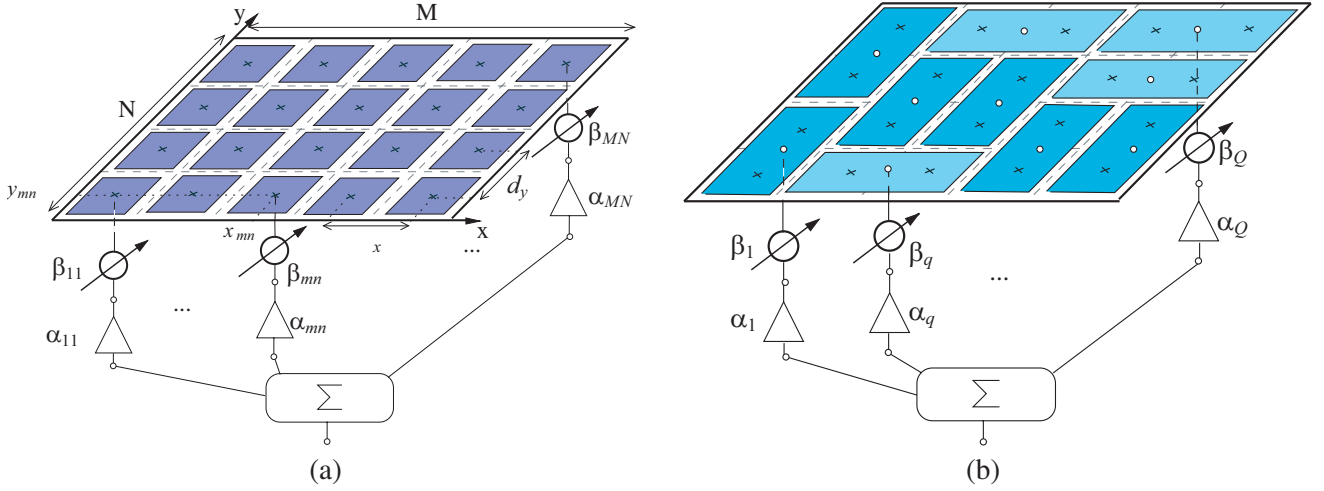
Figure 1. *Array Architecture* — Sketch of (a) the fully populated array architecture and (b) a domino tiled array of isotropic radiating elements.

populated array

$$w_{m,n} = \sum_{q=1}^{Q} \alpha_q e^{j\beta_q} \delta_{c_{m,n}q}, \quad n = 1, \ldots, N; \, m = 1, \ldots, M \tag{2}$$

where $\delta_{c_{m,n}q}$ is the Kronecker function ($\delta_{c_{m,n}q} = 1$ if $c_{m,n} = q$ and $\delta_{c_{m,n}q} = 0$, otherwise). With reference to this formulation, the mask-constrained synthesis of a domino tiled phased array can be formulated as follows:

Mask-Constrained Domino-Tiled Phased Array Design — Given an array of $M \times N$ elements located on a rectangular lattice, determine the optimal clustering of the array elements into vertical σ_V and horizontal σ_H domino tiles by defining the clustering vector $\underline{C}^{opt}$ and the corresponding sub-array level amplitude, $\underline{\alpha}^{opt} = \{\alpha_q^{opt}; \, q = 1, \ldots, Q\}$, and phase, $\underline{\beta}^{opt} = \{\beta_q^{opt}; \, q = 1, \ldots, Q\}$, excitation vectors so that the radiated power pattern has maximum directivity

$$D = \frac{4\pi \left| P\left(u_0, v_0; \underline{C}_t\right) \right|^2}{\displaystyle\int_{-1}^{1} \int_{-1}^{1} \left| P\left(u, v; \underline{C}_t\right) \right|^2 \frac{1}{\sqrt{1 - u^2 - v^2}} du \, dv} \tag{3}$$

along the direction of the mainlobe peak (u_0, v_0), subject to

$$P(u, v) \le M(u, v) \tag{4}$$

with $M(u, v)$ being a pattern mask mathematically defining the power requirements.

To solve such a synthesis problem, it is properly reformulated in an optimization one by defining the following cost function

$$\Phi\left(\underline{C}; \underline{\alpha}, \underline{\beta}\right) = \chi\left(\underline{C}; \underline{\alpha}, \underline{\beta}\right) + \frac{1 - \mathcal{H}\left[P(u, v) - M(u, v)\right]}{D(u_0, v_0)} \tag{5}$$

where $D(u_0, v_0)$ is the peak directivity, (u_0, v_0) the beam pointing direction, $\mathcal{H}[\cdot]$ the Heaviside function, and

$$\chi\left(\underline{C}; \underline{\alpha}, \underline{\beta}\right) = \max_{(u,v)\in\mathcal{V}} \left\{ \left| P(u, v) - M(u, v) \right| \mathcal{H}\left[P(u, v) - M(u, v)\right] \right\} \tag{6}$$

is the maximum violation of the power pattern from the power mask in the (u, v)-plane, within the visible region $\mathcal{V} = \{(u, v) : u^2 + v^2 < 1\}$. More in detail, the mask matching is quantified in terms of the maximum distance of the power pattern from the mask, $\chi(\underline{C}; \underline{\alpha}, \underline{\beta})$, only when the power pattern is above

the mask; otherwise, the cost function accounts only for the second term [i.e., the ratio $1/D(u_0, v_0)$] to maximize the peak directivity.

The global optimum of the mask-constrained domino tiling synthesis problem can be theoretically reached by means of a full-global optimization approach, by jointly optimize the tiling configuration $\underline{C}$ and the tiles excitations coefficients $\underline{\alpha}$ and $\underline{\beta}$, as

$$\left(\underline{C}^{opt}; \underline{\alpha}^{opt}, \underline{\beta}^{opt}\right) = \arg \left[\min_{\underline{C}, \underline{\alpha}, \underline{\beta}} \left\{\Phi\left(\underline{C}; \underline{\alpha}, \underline{\beta}\right)\right\}\right] \qquad (7)$$

Even for very small array, solving (7) turns out to be computationally intractable, because of the extremely wide solution space generated by setting $2Q$ real values (i.e., the values of the Q tiles amplitudes, α_q, $q = 1, \ldots, Q$, and phases, β_q, $q = 1, \ldots, Q$), and $M \times N$ integer numbers (i.e., the entries of the clustering vector, $c_{m,n}$, $m = 1, \ldots, M$, $n = 1, \ldots, N$). The main obstacle turns out to be the identification, among all the possible combinations of the integers $c_{m,n}$, $m = 1, \ldots, M$, $n = 1, \ldots, N$, of the admissible tiling configurations, $\underline{C}_t$, $t = 1, \ldots, T$, encoding the clustering of the $M \times N$ array elements into non-overlapping domino-like tiles. Towards this end, in [20] mathematical tiling theorems and algorithms [29, 32] are exploited to (i) verifying if rectangular array apertures are fully covered by the domino tiles [29], (ii) to know the exact number of existing domino tiling solutions T, analytically provided by the following closed-form formula [32]

$$T = 2^{\frac{MN}{2}} \prod_{m=1}^{M} \prod_{n=1}^{N} \left[\cos^2\left(\frac{\pi m}{M+1}\right) + \cos^2\left(\frac{\pi n}{N+1}\right)\right]^{1/4}, \qquad (8)$$

and (iii) to exactly generate the T different tiling configurations, $\underline{C}_t$, $t = 1, \ldots, T$, using the optimal domino-tiling method provided in [34]. Accordingly the mask-constrained synthesis method is addressed by using the Enumerative Tiling Method (ETM) presented in [20] for the joint optimization of the tilings $\underline{C}_t$, $t = 1, \ldots, T$ and of the sub-array coefficients, through a *nested optimization* strategy, in which the optimal tiling configuration is obtained as

$$\left(\underline{C}^{opt}; \underline{\alpha}^{opt}, \underline{\beta}^{opt}\right) = \arg \left[\min_{\underline{C}_t} \left\{\Phi\left(\underline{C}_t; \underline{\alpha}_t^{opt}, \underline{\beta}_t^{opt}\right); t = 1, \ldots, T\right\}\right] \qquad (9)$$

where the optimal excitations coefficients are optimized for each (t)-th ($t = 1, \ldots, T$) configuration as

$$\left(\underline{\alpha}_t^{opt}, \underline{\beta}_t^{opt}\right) = \arg \left[\min_{\underline{\alpha}_t, \underline{\beta}_t} \left\{\Phi\left(\underline{\alpha}_t, \underline{\beta}_t | \underline{C}_t\right)\right\}\right]; t = 1, \ldots, T \qquad (10)$$

In the following a set of methods, namely the *ETM-CP*, *EM-ETM/CP*, and *EM-OTM/CP*, implementing the nested optimization approach are described and discussed. Each method is proposed to solve a specific dimension of the problem, with the goal of providing the closest solution to the optimum, in a reasonable amount of time.

2.1. Enumerative CP-Optimized Method (ETM-CP)

In the case of small array size (e.g., $M < 6$, $N < 6$, $T < 100$) the nested optimization is implemented combining the enumeration of the tilings *(ETM)* with a Convex Programming (CP) optimization [35] of the tiles excitations coefficients in (10). The method, here named as *ETM-CP* approach, is described by the following procedural steps.

- **Step 1.** *Tilings Enumeration* — Execute the *ETM* method [20] to generate the whole set of admissible clustering configurations $\underline{C}_t$, $t = 1, \ldots, T$;
- **Step 2.** *CP Optimizations* — Given the power mask $M(u, v)$ defining the maximum upper bounds constraints on the power pattern, the following optimization problem is solved

$$\left(\underline{\alpha}_t^{CP}, \underline{\beta}_t^{CP}\right) = \arg \left[\min_{\underline{\alpha}_t, \underline{\beta}_t} \left\{\Phi\left(\underline{\alpha}_t, \underline{\beta}_t | \underline{C}_t\right)\right\}\right], t = 1, \ldots, T \qquad (11)$$

where for each tiling $\underline{C}_t$, $t = 1, \ldots, T$, the optimization of the sub-array weights is performed through the *CP* strategy presented in [35], in which the maximization of the power pattern directivity along the sum beam pointing direction is maximized, still satisfying the power mask $M(u, v)$. More in detail, the power mask $M(u, v)$ is uniformly discretized in R sampling directions, (u_r, v_r), $r = 1, \ldots, R$ and a standard *CP*-based optimization technique [35] is used to obtain the optimal subarray amplitude and phase excitations $(\underline{\alpha}_t^{CP}, \underline{\beta}_t^{CP})$ of the (t)-th $(t = 1, \ldots, T)$ trial clustering configuration $\underline{C}_t$, minimizing the cost function

$$\Psi\left(\underline{\alpha}_t, \underline{\beta}_t\right) = \int_{-1}^{1} \int_{-1}^{1} P(u, v; \underline{C}_t) \frac{1}{\sqrt{1 - u^2 - v^2}} du dv \qquad (12)$$
$$(u, v) \in \mathcal{V}$$

subject to the following constraints

$$P(u_0, v_0; \underline{C}_t) = 1 \qquad (13)$$

$$P(u, v; \underline{C}_t) \leq M(u_r, v_r) \qquad (14)$$
$$r = 1, \ldots, R$$

The minimization of (12) subject to (13) implies the maximization of the antenna directivity (3). If the mask constraints are too tight (i.e., no feasible solution to the problem exists) a sub-optimal solution must be obtained, for instance, by using interior-point algorithms [36] returning in these cases a minimizer, in the ℓ_1-norm, for the constraint violation, or by relaxing the mask until an optimal solution is found.

- **Step 3.** *Solution Selection* — Evaluate the cost function (5) for each *CP*-optimized solution, $\Phi(\underline{C}_t; \underline{\alpha}_t^{CP}, \underline{\beta}_t^{CP})$, $t = 1, \ldots, T$, and select the best tiling/sub-array weights as the one minimizing the cost, as

$$\left(\underline{C}^{ETM\text{-}CP}; \underline{\alpha}^{ETM\text{-}CP}, \underline{\beta}^{ETM\text{-}CP}\right) = \arg\left[\min_{\underline{C}_t; \underline{\alpha}_t^{CP}, \underline{\beta}_t^{CP}} \left\{\Phi\left(\underline{C}_t; \underline{\alpha}_t^{CP}, \underline{\beta}_t^{CP}\right); t = 1, \ldots, T\right\}\right] \qquad (15)$$

The computational time of the above procedure amounts to $\Delta t^{ETM\text{-}CP} = \Delta t^{ETM} + T \times \Delta t^{CP} + T \times \Delta t^{\Phi}$, where Δt^{ETM} is the time necessary to generate the configurations $\underline{C}_t$, $t = 1, \ldots, T$, Δt^{CP} the time of a single *CP* optimization, and Δt^{Φ} the time for the single evaluation of (5). It is worth noting here that the feasibility of the *ETM-CP* approach mainly depends on: (i) the cardinality of the solution space, T, and (ii) the computational cost needed to solve (10). Consequently, in the case of larger arrays, even if the enumeration of the T configurations would be possible within a reasonable time, the CP optimization time Δt^{CP} can make the approach computationally unfeasible.

2.2. Enumerative Excitation Matching Method (EM-ETM/CP)

In order to deal with medium sized arrays (e.g., $M < 10$, $N < 10$, $T < 1 \times 10^8$), the CP-based optimization of $(\underline{\alpha}_t, \underline{\beta}_t)$, $t = 1, \ldots, T$ is avoided substituting the *CP* method with an Excitation Matching (*EM*)-based approach. More in detail the *ETM* enumeration is combined with the analytic computation of the tiles excitations coefficients, minimizing the *EM* metric. Finally, the tiles excitation coefficients of the solution selected at the end of the process are optimized using CP. The proposed method, called *EM-ETM/CP*, is implemented throughout the following procedural steps:

- **Step 1.** *Reference Array* — Given the power mask $M(u, v)$ defining the ideal requirements on the power pattern, compute the optimal reference excitations weights $w^{Ref} = \alpha_{m,n}^{Ref} e^{j\beta_{m,n}^{Ref}}$, $m = 1, \ldots, M$; $n = 1, \ldots, N$ through a *CP* optimization of the $M \times N$ fully-populated array amplitude and phase coefficients [Fig. 1(a)];
- **Step 2.** *Tilings Enumeration* — Execute the *ETM* method [20] for the enumeration of the whole set of clustering configurations $\underline{C}_t$, $t = 1, \ldots, T$;

- **Step 3.** *EM Sub-Array Weights* — For each tiling $\underline{C}_t$, $t = 1, \ldots, T$, the optimal compromise *EM* amplitudes and phase coefficients $(\underline{\alpha}_t^{EM}, \underline{\beta}_t^{EM})$, $t = 1, \ldots, T$ are obtained solving the following excitation matching problem

$$\left(\underline{\alpha}_t^{EM}, \underline{\beta}_t^{EM}\right) = \arg\left[\min_{\underline{\alpha}_t, \underline{\beta}_t} \left\{ \sum_{m=1}^{M} \sum_{n=1}^{N} \left| w_{m,n}^{Ref} - w_{m,n,t}^{EQ} \right| \right\}\right]; \; t = 1, \ldots, T \qquad (16)$$

whose solution, turns out to be analytically obtained as [9]

$$\alpha_{q,t}^{EM} = \frac{1}{2} \sum_{n=1}^{N} \sum_{m=1}^{M} \alpha_{m,n}^{Ref} \delta_{c_{m,n,t}q}, \quad q = 1, \ldots, Q; \; t = 1, \ldots, T \qquad (17)$$

$$\beta_{q,t}^{EM} = \frac{1}{2} \sum_{n=1}^{N} \sum_{m=1}^{M} \beta_{m,n}^{Ref} \delta_{c_{m,n,t}q}, \quad q = 1, \ldots, Q; \; t = 1, \ldots, T \qquad (18)$$

- **Step 4.** *Cost Function Evaluation* — Evaluate the cost function (5) for each T solutions and select the best tiling/sub-array weights, solving

$$\underline{C}^{EM\text{-}ETM} = \arg\left[\min_{\underline{C}_t} \left\{ \Phi\left(\underline{C}_t; \underline{\alpha}_t^{EM}, \underline{\beta}_t^{EM}\right); \; t = 1, \ldots, T \right\}\right] \qquad (19)$$

- **Step 5.** *CP Optimization* — The amplitude and phase tiles excitations of the selected *EM-ETM* solution, $\underline{C}^{EM-ETM}$, are finally optimized using a *CP* optimization in order to completely fulfill the mask constraints

$$\left(\underline{\alpha}^{EM\text{-}ETM/CP}, \underline{\beta}^{EM\text{-}ETM/CP}\right) = \arg\left[\min_{\underline{\alpha}, \underline{\beta}} \left\{ \Phi\left(\underline{\alpha}, \underline{\beta} \,\middle|\, \underline{C}^{EM\text{-}ETM}\right) \right\}\right] \qquad (20)$$

In this case, the total computational time equals $\Delta t^{EM\text{-}ETM/CP} = \Delta t^{ETM} + T \times \Delta t^{EM} + T \times \Delta t^{\Phi} + 2 \times \Delta t^{CP}$, where Δt^{EM} is the time necessary for the *EM* excitation computation. The use of the analytic formulas (17) and (18) allows a fast computation of the tiles excitations weights, thus enabling the synthesis of larger array sizes with respect to the *ETM-CP* approach, while the computational time is only limited by T. Accordingly, in the case of large arrays, [e.g., $M > 10$, $N > 10$], the EM-ETM/CP turns out to be computationally intractable.

2.3. Excitation Matching Optimization Method (EM-OTM/CP)

When the number of solutions, T, is large enough (e.g., $T \geq 1 \times 10^6$) to make both *ETM-CP* and *EM-ETM/CP* methods unfeasible, the *OTM* methodology presented in [20] is here used to efficiently explore a subset of the whole set of tilings. The *OTM* proposed in [20] exploits a schemata-driven *GA*, in which the probability to converge towards solutions that are very close to the global optimum is enhanced by a smart initialization of the optimizer. The strategy proposed for solving the mask constrained synthesis problem inherits from the *EM-ETM/CP* approach (i) the computation of the tiles amplitudes and phase coefficients, $\underline{\alpha} = \{\alpha_q; q = 1, \ldots, Q\}$, $\underline{\beta} = \{\beta_q; q = 1, \ldots, Q\}$, minimizing the *EM* metric using (17) and (18); and (ii) the final *CP* optimization of the tiles excitations coefficients for the *EM-OTM* solution. More in detail, the *OTM* strategy presented in [20] exploits the efficient height-function (*HF*)-based coding [33, 34] of the T domino tilings into words of $L < (M \times N)$ integer values, $\underline{w}_t = \{w_{l,t} \in [w_{l,1} \div w_{l,T}]; l = 1, \ldots, L\}$, $t = 2, \ldots, T - 1$, starting from the knowledge of *a-priori* and analytically defined tiling words, $\underline{w}_1$ and $\underline{w}_T$. Accordingly, the GA is initialized with a population of U trial individuals/solutions $\underline{w}_u$, $u = 1, \ldots, U$, selected using the schemata-driven method [20] and encoded into binary chromosomes $\widehat{\underline{w}}_u$, $u = 1, \ldots, U$. The successive generations of populations are obtained iteratively applying the standard *GA* operators, namely the *roulette-wheel* selection, the *single-point crossover*, and the *mutation* [37], using the *EM* technique for the computation of the tiles amplitude and phase coefficients, until a tiling solution that completely fulfills the mask constraints

$M(u, v)$ is generated [i.e., $\chi(\underline{C}^{EM\text{-}OTM}; \underline{\alpha}^{EM\text{-}OTM}, \underline{\beta}^{EM\text{-}OTM}) = 0$] or when the maximum number of iterations, K, is reached. Finally, the optimal sub-array weights are obtained as:

$$\left(\underline{\alpha}^{EM\text{-}OTM/CP}, \underline{\beta}^{EM\text{-}OTM/CP} \right) = \arg \left[\min_{\underline{\alpha}, \underline{\beta}} \left\{ \Phi \left(\underline{\alpha}, \underline{\beta} \, | \, \underline{C}^{EM\text{-}OTM} \right) \right\} \right]. \tag{21}$$

3. NUMERICAL VALIDATION

In this section, the numerical validation considering different array dimensions, as well as different types of synthesis mask, is reported. A set of examples showing the different ranges of applicability of the proposed methods, when small, medium, and large array sizes are considered, are illustrated and discussed. Finally, the reliability assessment of the optimized solutions when considering real radiating elements is reported.

3.1. Small Dimensions Arrays

Let us consider a small rectangular aperture of dimensions $2.5\lambda \times 2.0\lambda$, filled by $M \times N = 5 \times 4$ elements, located over a square lattice, equally spaced by $d_x = d_y = \lambda/2$. The ideal design requirements are defined by the power mask $M(u, v)$ of Fig. 2(a), characterized by a rectangular window of dimension $BW_u \times BW_v = 1.00\,[u] \times 1.12\,[v]$ for the main beam, a sidelobe level equal to $SLL_{L1} = -20\,[\text{dB}]$ for the first sidelobes, while the end-fire sidelobes along the azimuth plane are lowered to $SLL_{L2} = -25\,[\text{dB}]$. The fully populated reference array phase coefficients are set to $\beta_{m,n}^{Ref} = 0$, $m = 1, \ldots, M$, $n = 1, \ldots, N$, while the amplitude coefficients have been optimized using the max-directivity CP optimization [35], setting a maximum number of iterations equal to $I = 200$ and a convergence threshold equal to $\tau = 10^{-6}$.
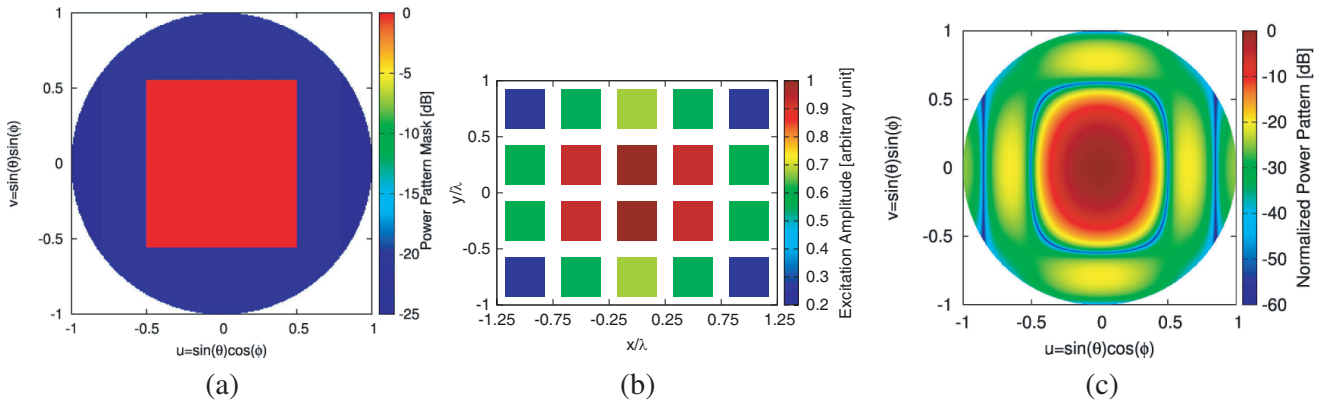

(a) (b) (c)

Figure 2. *Numerical Assessment (Small Array, Symmetric Mask; $d = 0.5\lambda$, $M \times N = 5 \times 4$ $N_{tot} = 20$) — The reference solution of the fully-populated array obtained through a CP optimization.* (a) The power mask, (b) the amplitude coefficients, and (c) the top-view power pattern.

The obtained amplitude coefficients are shown in Fig. 2(b), and the corresponding power pattern is reported in Fig. 2(c). According to (8), the array allows to entirely cover the aperture with $Q = 15$ tiles in $T = 95$ different ways. Consequently, the limited number of tiling configurations enable the use of the $ETM\text{-}CP$ approach. The simulation takes a total amount of time equal to 9 [hours] 44 [min] and 30 [sec] considering the same CP parameters used for the reference array synthesis. Fig. 3(a) shows the values of the mask matching cost function term of the T solutions sorted from the best to the worst one. In order to discriminate among the convergent solutions fitting the mask with cost-function value lower than the threshold and the solutions that violates the mask, the CP convergence threshold is reported in the figure as a black dashed line. As can be seen, 6 $ETM\text{-}CP$ solutions have a mask violation value that is below the convergence threshold, among which the one minimizing the mask violation is reported in Figs. 4(a)–(b) whose respective power pattern descriptors, namely the SLL,
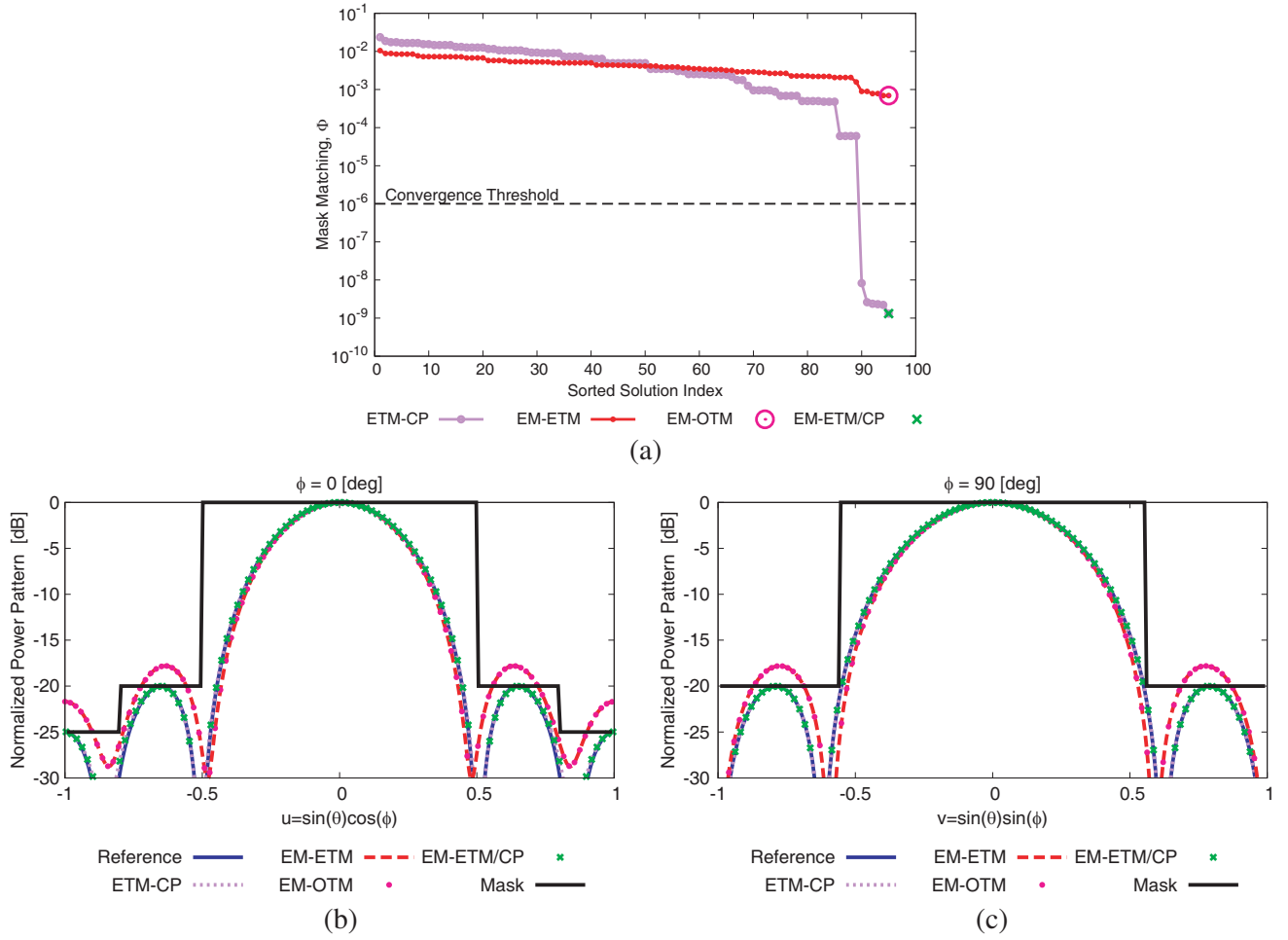
Figure 3. *Numerical Assessment* (*Small Array, Symmetric Mask*; $d = 0.5\lambda$, $M \times N = 5 \times 4$ $N_{tot} = 20$, $T = 95$) — (a) The *ETM-CP* cost function evaluations for each of the $T = 95$ tiling solutions, as compared to the *EM-ETM* simulation cost function evaluations, and the cost function of the *EM-ETM/CP* simulation. (b) (c) The power pattern cuts along the $u = u_0 = 0.0$ and $v = v_0 = 0.0$ plane of the *ETM-CP*, the *EM-ETM*, and the *EM-OTM* optimal solutions and the *EM-ETM/CP* solution, as compared to the power mask.

$HPBW_{AZ}$, $HPBW_{EL}$, and D, are reported in Table 1. The comparisons of the power pattern with the power mask of the optimal *ETM-CP* solution are reported in Fig. 3(b) and Fig. 3(c), along the azimuth and elevation planes, respectively. As can be seen, the pattern meets the mask, also confirmed by the final cost function value [$\Phi^{ETM-CP} = 1.22 \times 10^{-9}$, Table 1].

The same test case is considered to validate the *EM*-based nested approaches (*EM-ETM/CP* and *EM-OTM/CP*), in order to check the closeness to the optimal *ETM-CP* solution. Accordingly, the *EM-ETM* optimization has been executed considering reference excitations equal to the CP amplitudes coefficients of Fig. 2(a). The evaluated cost function values have been reported in Fig. 3(a) as compared to the *ETM-CP* method; however, none of the *EM-ETM* solutions reach the convergence threshold, showing a non-negligible distance of the *EM-ETM* best solution from the *ETM-CP* one. Indeed, by observing Figs. 3(b)–(c) the power pattern cuts along the azimuth and elevation planes of the *EM-ETM* power pattern violates the power mask in both the principal planes cuts. Anyway, by observing the tiling/amplitudes configuration of the best *EM-ETM* solution [Figs. 4(c)–(d)], the tiles arrangement is exactly the same as the *ETM-CP* tiling [Fig. 4(a)], while the sub-array amplitude coefficients show different values. Finally, the optimal *ETM-CP* solution is obtained after a *CP* optimization of the tiles amplitudes [Figs. 4(e)–(f)], thus making the *EM-ETM/CP* method converge to the *ETM-CP* solution
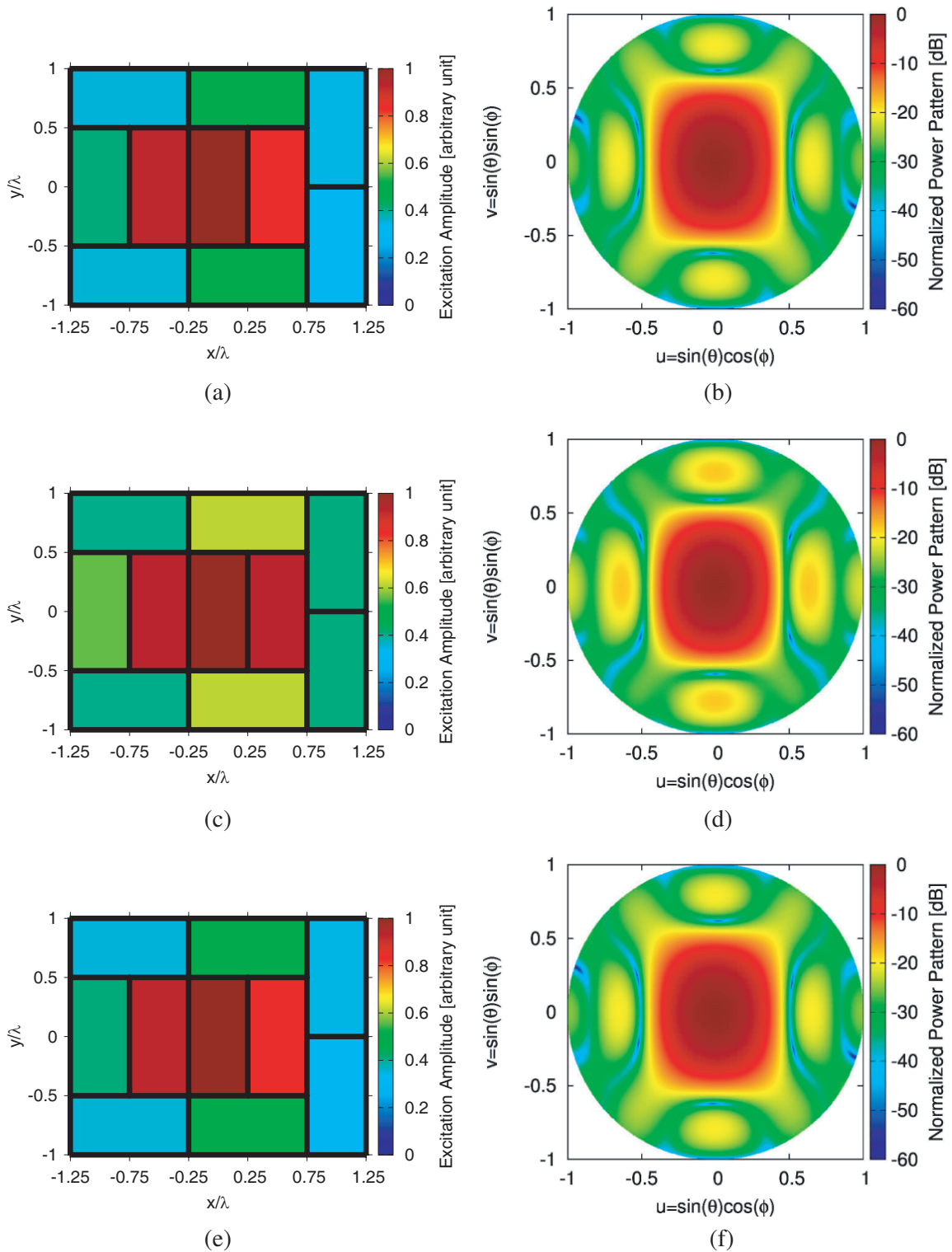
Figure 4. *Numerical Assessment* (*Small Array, Symmetric Mask*; $d = 0.5\lambda$, $M \times N = 5 \times 4$ $N_{tot} = 20$, $T = 95$) — (a) (c) (e) The tiles amplitudes excitations coefficients and (b) (d) (f) the respective top-view power patterns of the (a) (b) *ETM-CP* optimal solution, (c) (d) the *EM-ETM* optimal solution, and the (e) (f) *EM-ETM/CP* solution.

Table 1. *Numerical Assessment (Small Array, Symmetric Mask*; $d = 0.5\lambda$, $M \times N = 5 \times 4$ $N_{tot} = 20$, $T = 95$*)* — Measured radiation indexes (SLL, D, $HPBW_{az}$, and $HPBW_{el}$), and cost function Φ of the reference and optimized tilings patterns, and timings of the optimizations/simulations.

	SLL [dB]	D [dBi]	$HPBW_{az}$ [deg]	$HPBW_{el}$ [deg]	Φ -	Δt [h : min : sec]
			$M \times N = 4 \times 5\ Symmetric\ Mask$			
Reference	-20.00	17.12	24.15	30.10	2.36×10^{-9}	$00 : 11 : 40$
ETM-CP	-20.00	16.95	24.21	30.10	1.22×10^{-9}	$09 : 44 : 30$
EM-ETM	-17.80	17.20	23.49	29.29	6.94×10^{-4}	$00 : 00 : 31$
EM-OTM	-17.80	17.20	23.49	29.29	6.94×10^{-4}	$00 : 00 : 05$
EM-ETM/CP	-20.00	16.95	24.21	30.10	1.22×10^{-9}	$00 : 00 : 47$

[Fig. 4(a)]. It is worth noting here that the overall time needed to obtain the global optimum using the *EM-ETM/CP* method has been estimated equal to $\Delta t^{EM\text{-}ETM/CP} = \Delta t^{Ref} + \Delta t^{EM\text{-}ETM} + \Delta t^{CP} = 1 : 18\,[\text{min} : \text{sec}]$ (Table 1), which means a time reduction of 99.7% with respect to the *ETM-CP* approach. With the purpose of validating the *EM-OTM/CP* strategy, the *GA*-based schemata-driven optimization presented in [20] has also been executed. The *GA* control parameters have been set according to the rules described in [20] ($U = 6$, $K = 10$, crossover probability $p_c = 0.9$, and mutation probability $p_m = 0.01$). For statistical reasons, the *GA* optimization has been executed for 10 different times, always converging to the *EM-ETM/CP* solution [Figs. 3(b)–(c)].

3.2. Medium Dimensions Arrays

In order to assess the proposed methodology for small/medium sized arrays, a $4.5\lambda \times 3\lambda$ rectangular aperture is now considered, filled with $N \times M = 9 \times 6$ elements located over a squared lattice and equally spaced by $d_x = d_y = \lambda/2$. The symmetric power mask of Fig. 5(a) defines the optimal pattern shape, consisting in a main beam window of dimension $BW_u \times BW_v = 0.5\,[u] \times 0.8\,[v]$, a maximum $SLL_{L1} = -20\,[\text{dB}]$ for the lobes nearby the main lobe, and a maximum $SLL_{L2} = -25\,[\text{dB}]$ in the end-fire zone. The *CP* optimized amplitude coefficients of the reference fully-populated array, together with the synthesized power pattern, are reported in Fig. 5. According to (8), an $M \times N = 9 \times 6$ elements array can be partitioned into exactly $T = 8.17991 \times 10^5$ different tilings. It is clear that in this case the amount of time needed to complete *ETM-CP* simulations turns out to be very large (i.e., $\Delta t \simeq 94$ days, assuming $\Delta t^{CP} \simeq 10\,[\text{sec}]$). The *EM*-based techniques instead allow to complete the optimization into a reasonable amount of time (i.e., $\Delta t^{EM\text{-}ETM} = 15 : 39 : 36\,[\text{h} : \text{min} : \text{sec}]$ and $\Delta t^{EM\text{-}OTM} = 00 : 20 : 12\,[\text{h} : \text{min} : \text{sec}]$, Table 3).

Table 2. *Numerical Assessment (Medium Array, Symmetric Mask*; $d = 0.5\lambda$, $M \times N = 6 \times 9$ $N_{tot} = 54$, $T \simeq 8.2 \times 10^5$*)* - Measured radiation indexes (SLL, D, $HPBW_{az}$, and $HPBW_{el}$), and cost function Φ of the reference and optimized tilings patterns, and timings of the optimizations/simulations.

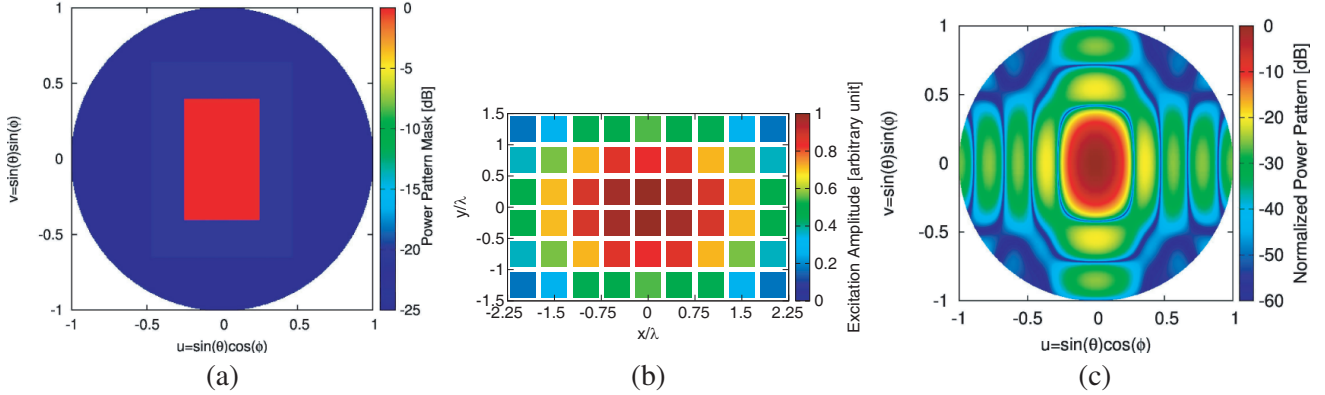|	SLL [dB]	D [dBi]	$HPBW_{az}$ [deg]	$HPBW_{el}$ [deg]	Φ -	Δt [h : min : sec]
			$M \times N = 6 \times 9\ Symmetric\ Mask$			
Reference	-20.00	21.52	13.15	20.07	3.60×10^{-10}	$00 : 21 : 25$
EM-ETM	-19.11	21.54	13.03	19.86	4.80×10^{-5}	$15 : 39 : 36$
EM-OTM	-19.11	21.54	13.03	19.86	4.80×10^{-5}	$00 : 20 : 12$
EM-ETM/CP	-20.00	21.46	13.15	20.07	5.00×10^{-10}	$00 : 03 : 30$

Figure 5. *Numerical Assessment (Medium Array, Symmetric Mask; $d = 0.5\lambda$, $M \times N = 6 \times 9$ $N_{tot} = 54$) — The reference solution of the fully-populated array obtained through a CP optimization. (a) The synthesis mask, (b) the amplitude coefficients, and (c) the top-view power pattern.*

The cost-function evaluated by the *EM-ETM* for all the existing tilings has been reported in Fig. 6(a), together with the best solution provided by the *EM-OTM* approach using the following parameters: $U = 54$, $K = 500$, $p_c = 0.9$, $p_m = 0.01$. It is worth noting that also in this case the *EM-OTM* method achieves the same *EM-ETM* solution. Fig. 7(a) reports the respective tiling, as well as the amplitude coefficients while the top-view power pattern is shown in Fig. 7(b). The comparison of the power pattern with the power mask is reported in Figs. 6(b)–(c) along the azimuth and elevation planes, respectively. As can be seen, the power pattern corresponding to the *EM-ETM* solution does not match the optimal performances [$\Phi^{EM\text{-}ETM} = 4.8 \times 10^{-5}$, Table 2]. Nevertheless, the solution obtained through the proposed *EM/ETM-CP* method [Figs. 7(c)–(d)] affords a power pattern that completely fits the power mask, as confirmed by the final cost function value [$\Phi^{EM\text{-}ETM/CP} = 5.0 \times 10^{-10}$, Table 2], which is below the convergence threshold [Fig. 6(a)].

Table 3. *Numerical Assessment (Medium Array, Asymmetric Mask; $d = 0.5\lambda$, $M \times N = 6 \times 9$ $N_{tot} = 54$, $T \simeq 8.2 \times 10^5$) — Measured radiation indexes (SLL, D, $HPBW_{az}$, and $HPBW_{el}$), and cost function Φ of the reference and optimized tilings patterns, and timings of the optimizations.*

	SLL	D	$HPBW_{az}$	$HPBW_{el}$	Φ	Δt
	[dB]	[dBi]	[deg]	[deg]	-	[h : min : sec]
	$M \times N = 6 \times 9$ *Asymmetric Mask*					
Reference	-25.00	20.81	14.53	21.61	3.05×10^{-10}	$00:27:35$
EM-ETM	-23.48	20.85	14.32	21.33	2.40×10^{-4}	$16:08:10$
EM-OTM	-23.48	20.85	14.32	21.33	2.40×10^{-4}	$00:25:20$
EM-ETM/CP	-24.45	20.63	14.69	21.49	1.70×10^{-5}	$01:47:46$

In order to show the versatility of the proposed methodologies, a second assessment of the 9×6 array has been performed considering the asymmetric mask of Fig. 8(d). A window of dimension $BW_u \times BW_v = 0.64\,[u] \times 0.92\,[v]$ is considered for the main beam, while three different SLL levels are asymmetrically defined in the side-lobes zone: $SLL_{L1} = -25\,[\text{dB}]$, $SLL_{L2} = -28\,[\text{dB}]$, and $SLL_{L3} = -35\,[\text{dB}]$. The reference complex excitations of the fully populated array are reported in Figs. 8(a)–(b) and the corresponding power pattern in Fig. 8(c). As shown in Fig. 9(a), the *EM-ETM* and *EM-OTM* simulations converge to the same *EM*-optimal solution showing a mask matching equal to $\Phi^{EM-ETM} = 2.4 \times 10^{-4}$ (Tab. 3), whose corresponding tiling is pictured in Figs. 10(a)–(b), together with the *EM-ETM* amplitude and phase coefficients, while the top view power pattern is reported in
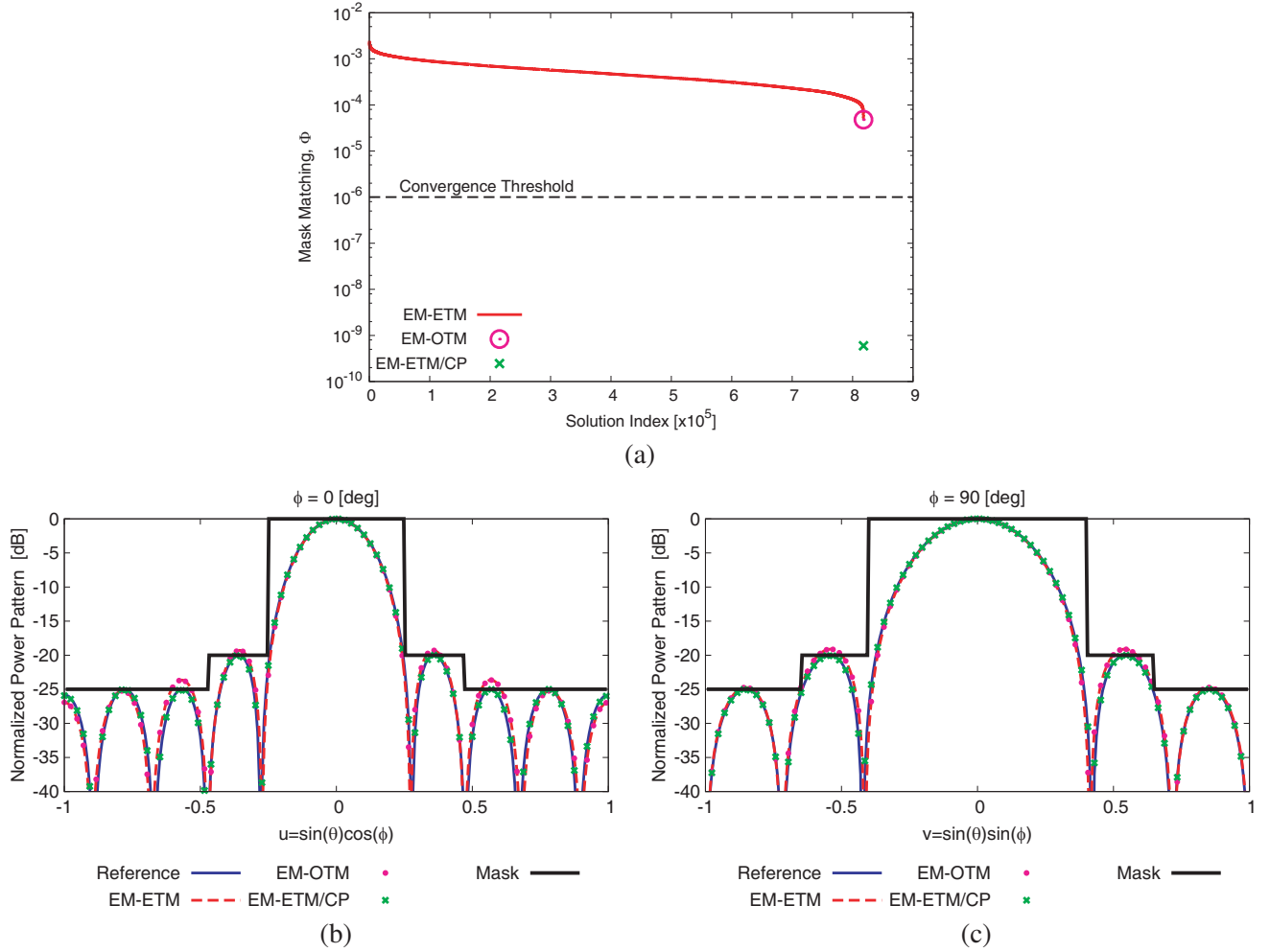
Figure 6. *Numerical Assessment (Medium Array, Symmetric Mask*; $d = 0.5\lambda$, $M \times N = 6 \times 9$ $N_{tot} = 54$) — *Numerical Assessment (Medium Array, Symmetric Mask*; $d = 0.5\lambda$, $M \times N = 6 \times 9$ $N_{tot} = 54$, $T \simeq 8.2 \times 10^5$) — (a) The *EM-ETM*, and the *EM-OTM* simulation cost function evaluations, and the cost function of the *EM-ETM/CP* simulation. (b)–(c) The power pattern cuts along the $u = u_0 = 0.0$ and $v = v_0 = 0.0$ plane of the *EM-ETM*, and the *EM-OTM* optimal solution and the *EM-ETM/CP* solution, as compared to the reference fully-populated solution and to the power mask.

Fig. 10(c). The *EM-ETM/CP* optimized solution [Figs. 10(d)–(f)] still does not reach the convergence. Consequently, the cost function value [$\Phi^{EM-ETM/CP} = 1.7 \times 10^{-5}$, Table 3] is still above the convergence threshold [Fig. 9(a)], but it is lower than the *EM-ETM* solution. Indeed, even if the *EM-ETM/CP* power pattern violates the power mask [Figs. 9(b)–(c)], the corresponding beam pattern descriptors (Table 3) are very close to the optimal ones ($\Delta SLL = |SLL^{EM-ETM/CP} - SLL^{Ref}| = 0.55$ [dB], $\Delta D = |D^{EM-ETM/CP} - D^{Ref}| = 0.18$ [dBi], $\Delta HPBW_{AZ} = |HPBW_{AZ}^{EM-ETM/CP} - HPBW_{AZ}^{Ref}| = 0.16$ [deg], $\Delta HPBW_{EL} = |HPBW_{EL}^{EM-ETM/CP} - HPBW_{EL}^{Ref}| = 0.12$ [deg]). In order to quantify the robustness of the optimized tiled array, when the beam is steered off-broadside directions, the mask matching of the power pattern varying the beam pointing within the visible range (i.e., $0° \leq \theta_0 < 90°$ and $0° \leq \phi_0 < 360°$) has been evaluated and reported in the polar diagram of Fig. 11(a). It can be noticed that the steering of the beam along the $\phi_0 = 90$ [deg] direction leads to higher mask matching values than the steering along the azimuth plane. A detail of the steering analysis is reported in Fig. 11(b), which shows the mask matching as a function of the pointing angle θ_0 along the $\phi_0 = 0$ [deg] and $\phi_0 = 90$ [deg] planes.
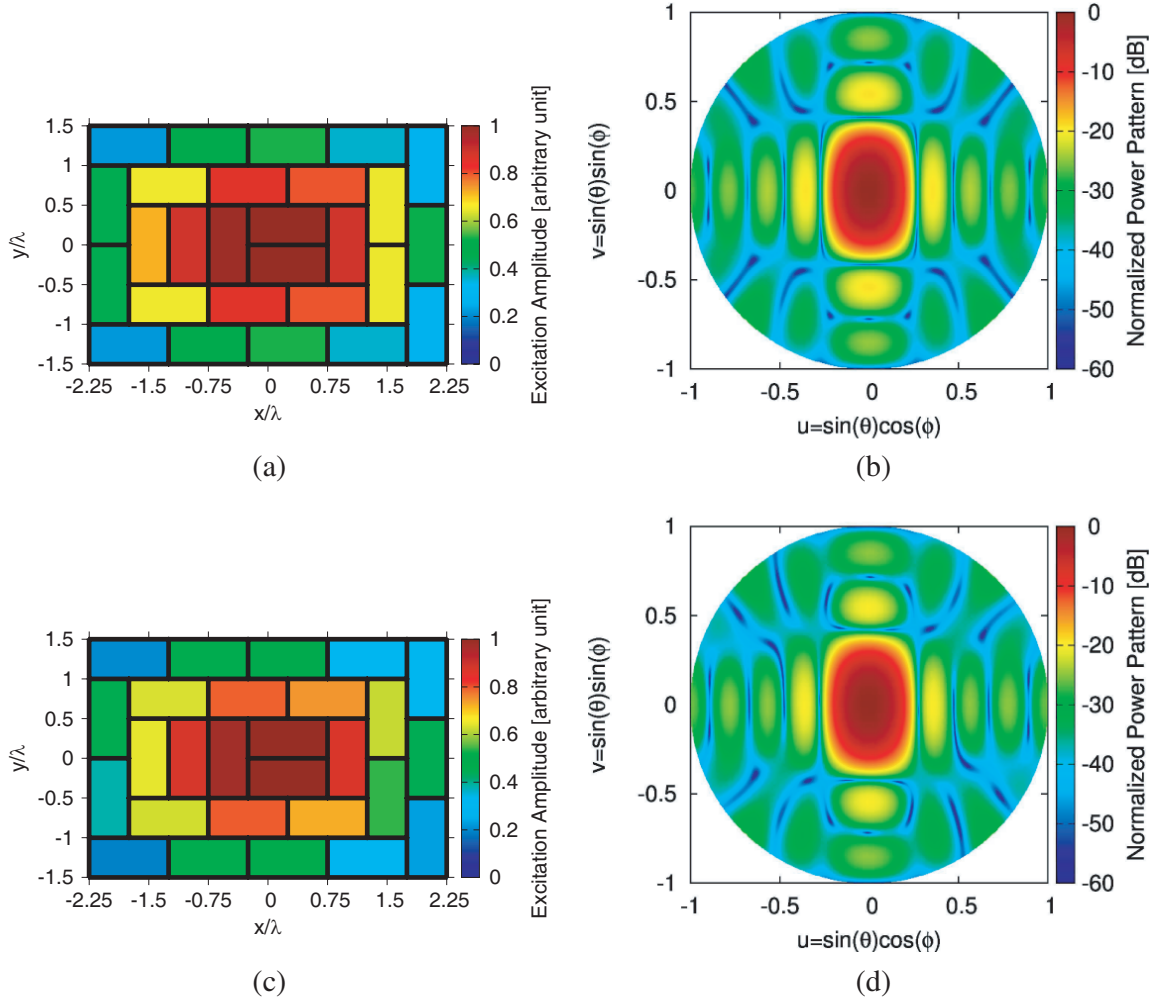
(a)

(b)

(c)

(d)

Figure 7. *Numerical Assessment (Medium Array, Symmetric Mask; $d = 0.5\lambda$, $M \times N = 6 \times 9$ $N_{tot} = 54$, $T \simeq 8.2 \times 10^5$) — (a) (c) The tiles amplitudes excitations coefficients and (b) (d) the respective top-view power patterns of the (a) (b) EM-ETM optimal solution, and (c) (d) the EM-ETM/CP solution.*

3.3. Large Dimensions Arrays

As a final example, a larger array is considered. The array aperture is a rectangle of dimension $10\lambda \times 7.5\lambda$ filled by $N_{tot} = 300$ elements located over a 20×15 grid, equally spaced by $d_x = d_y = \lambda/2$. The considered power mask is shown in Fig. 12. As can be seen, the mask is asymmetric with a main beam window of dimension $BW_u \times BW_v = 0.32\,[u] \times 0.42\,[v]$ and SLL levels equal to: $SLL_{L1} = -25\,[\text{dB}]$, $SLL_{L2} = -30\,[\text{dB}]$, and $SLL_{L3} = -40\,[\text{dB}]$.

Figures 12(a)–(b) show the optimal CP excitation coefficients of the reference fully-populated array, while Fig. 12(c) shows the top view of the synthesized power pattern. In this case, the cardinality of the solution space equals $T = 4.9098 \times 10^{35}$, which is too large for an exhaustive exploration, and consequently, the EM-OTM has been chosen in order to search for the optimal tiling in a feasible amount of time. Indeed, 10 different GA optimizations have been executed considering $U = 800$ individuals, $K = 1000$ iterations, $p_c = 0.9$, and $p_m = 0.01$, for a total simulation time equal to $\Delta t = 16 : 42 : 30\,[\text{h}:\text{min}:\text{sec}]$. The fitness of all the executed simulations is reported in Fig. 13(a) as function of the iteration index. As can be seen, all the GA simulations converge to cost-functions values within the interval $[2.0 \times 10^{-6}, 1.8 \times 10^{-6}]$. The 50% of the executed GA simulations converge to the same best solution having a matching with the mask equal to $\Phi(\underline{C}^{EM\text{-}OTM}; \underline{\alpha}^{EM\text{-}OTM}, \underline{\beta}^{EM\text{-}OTM}) = 1.8 \times 10^{-6}$ (Table 4). The EM-optimal tiling, together with
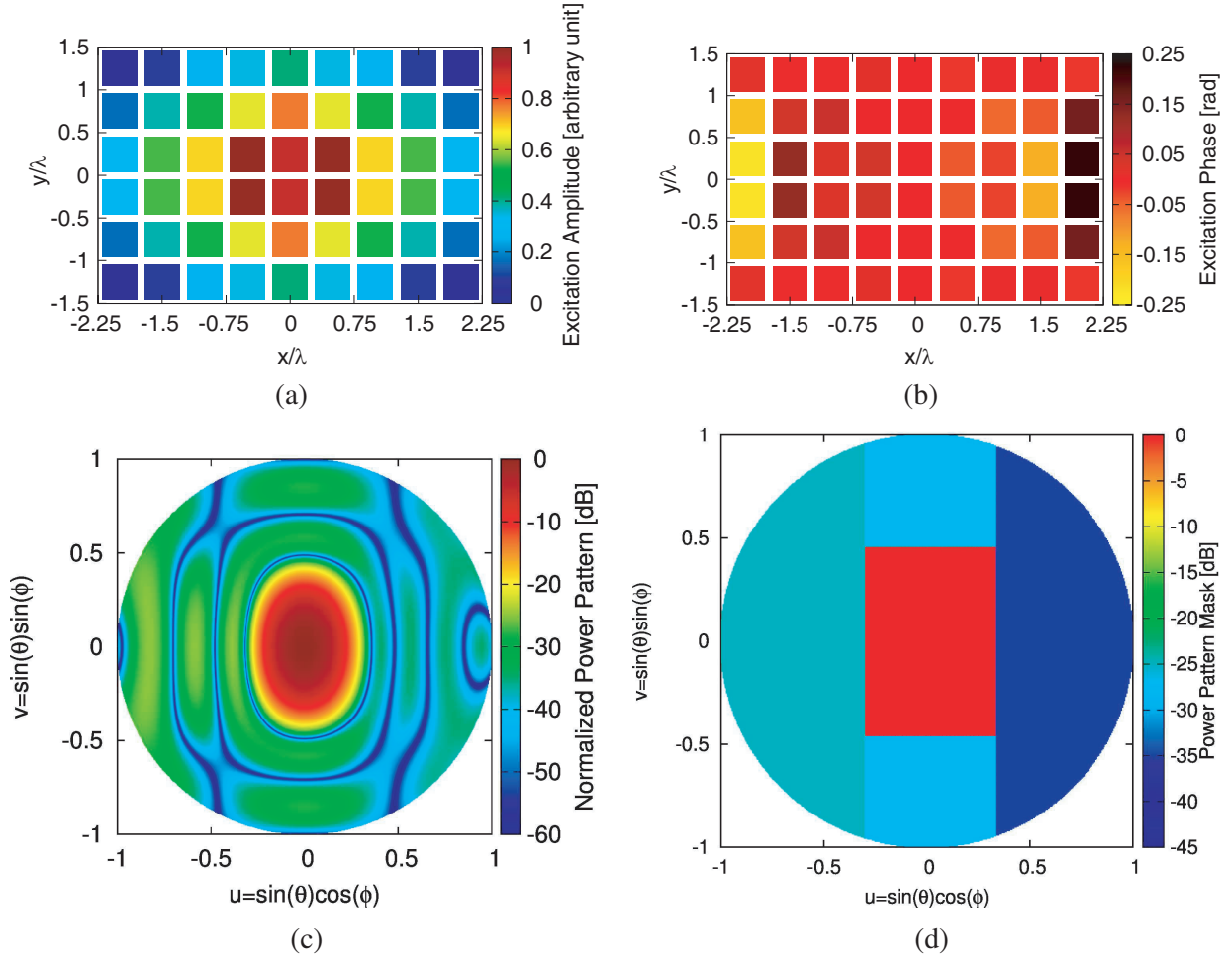
(a)

(b)

(c)

(d)

Figure 8. *Numerical Assessment (Medium Array, Asymmetric Mask*; $d = 0.5\lambda$, $M \times N = 6 \times 9$ $N_{tot} = 54$, $T \simeq 8.2 \times 10^5$*)* — The reference solution of the fully-populated array obtained through a *CP* optimization. (a) The amplitude coefficients, (b) the phase coefficients, (c) the top-view power pattern, and (d) the synthesis mask.

the amplitude and phase excitation coefficients, is reported in Figs. 14(a)–(b), respectively, while the top view power pattern is reported in Fig. 14(c). Even if the *EM-OTM* solution does not match the mask completely, the *EM-OTM/CP* solution [Figs. 14(d)–(f)] successfully lowers the mask matching below the convergence threshold [$\Phi(\underline{C}^{EM-OTM/CP}; \underline{\alpha}^{EM-OTM/CP}, \underline{\beta}^{EM-OTM/CP}) = 6.2 \times 10^{-9}$, Table 4] as also confirmed by the comparison of the power pattern cuts along the $u = u_0 = 0.0$ and $v = v_0 = 0.0$ planes [Figs. 13(b)–(c)]. The analysis of the optimized tiled array, when the beam is steered off-broadside directions, is reported in Fig. 15 in terms of mask matching.

In order to check the flexibility of the optimized domino tiling configurations, the tiling solution optimized to fit at best the mask of Fig. 12(d) has been analyzed changing the amplitude tapering distribution. More in detail the tiling configuration has been fixed to be equal to the EM-OTM optimized solution of Fig. 14(a), while the amplitude tapering has been set equal to the Dolph-Chebyshev distribution of Fig. 16(a) generating a reference beam with equi-ripple sidelobes with $SLL = -30$ [dB] and fitting the radiation mask reported in Figs. 16(d)–16(e). Fig. 16(b) shows the sub-array configuration together with the new clustered amplitude coefficients, while the corresponding pattern is compared to the reference pattern and the mask along the main planes in Figs. 16(d)–16(e). The mask deviation amounts to $\Phi = 3.73 \times 10^{-6}$, which is slightly higher than the EM-OTM solution when considering the asymmetric mask (i.e., $\Phi = 1.8 \times 10^{-6}$, Table 4) but with the same
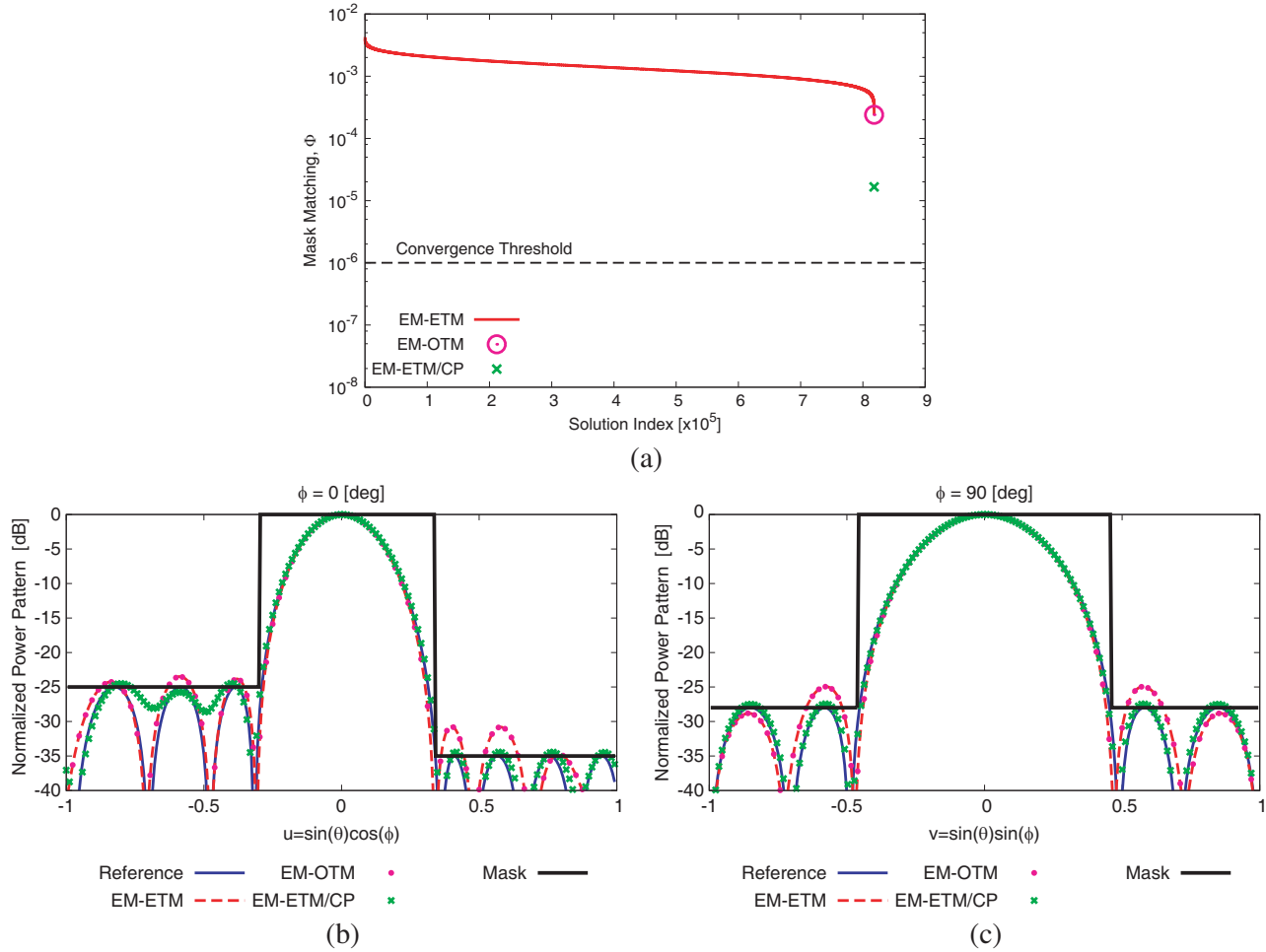
Figure 9. *Numerical Assessment (Medium Array, Asymmetric Mask; $d = 0.5\lambda$, $M \times N = 6 \times 9$ $N_{tot} = 54$, $T \simeq 8.2 \times 10^5$) — (a) The EM-ETM, and the EM-OTM simulation cost function evaluations, and the cost function of the EM-ETM/CP simulation. (b)–(c) The power pattern cuts along the $u = u_0 = 0.0$ and $v = v_0 = 0.0$ plane of the The EM-ETM, and the EM-OTM optimal solution and the EM-ETM/CP solution, as compared to the reference fully-populated solution and to the power mask.*

Table 4. *Numerical Assessment (Medium Array, Asymmetric Mask; $d = 0.5\lambda$, $M \times N = 6 \times 9$ $N_{tot} = 54$, $T \simeq 8.2 \times 10^5$) — Measured radiation indexes (SLL, D, $HPBW_{az}$, and $HPBW_{el}$), and cost function Φ of the reference and optimized tilings patterns, and timings of the optimizations.*

	SLL	D	$HPBW_{az}$	$HPBW_{el}$	Φ	Δt
	[dB]	[dBi]	[deg]	[deg]	-	[h : min : sec]
	$M \times N = 15 \times 20$ *Asymmetric Mask*					
Reference	-25.00	28.27	6.50	8.60	9.57×10^{-9}	$02 : 59 : 03$
EM-OTM	-24.73	28.31	6.48	8.56	1.80×10^{-6}	$04 : 28 : 29$
EM-OTM/CP	-25.00	28.24	6.51	8.60	6.20×10^{-9}	$02 : 07 : 07$

order of magnitude, as also confirmed by Figs. 16(d)–16(e) showing small pattern deviations only along the $\phi_0 = 90$ [deg] plane. For comparison, a trivial regular domino tiling configuration has also been considered [Fig. 16(c)], showing in this case larger mask deviations ($\Phi = 3.78 \times 10^{-5}$) and high side lobes mainly in the end-fire region along the $\phi_0 = 0$ [deg] plane.
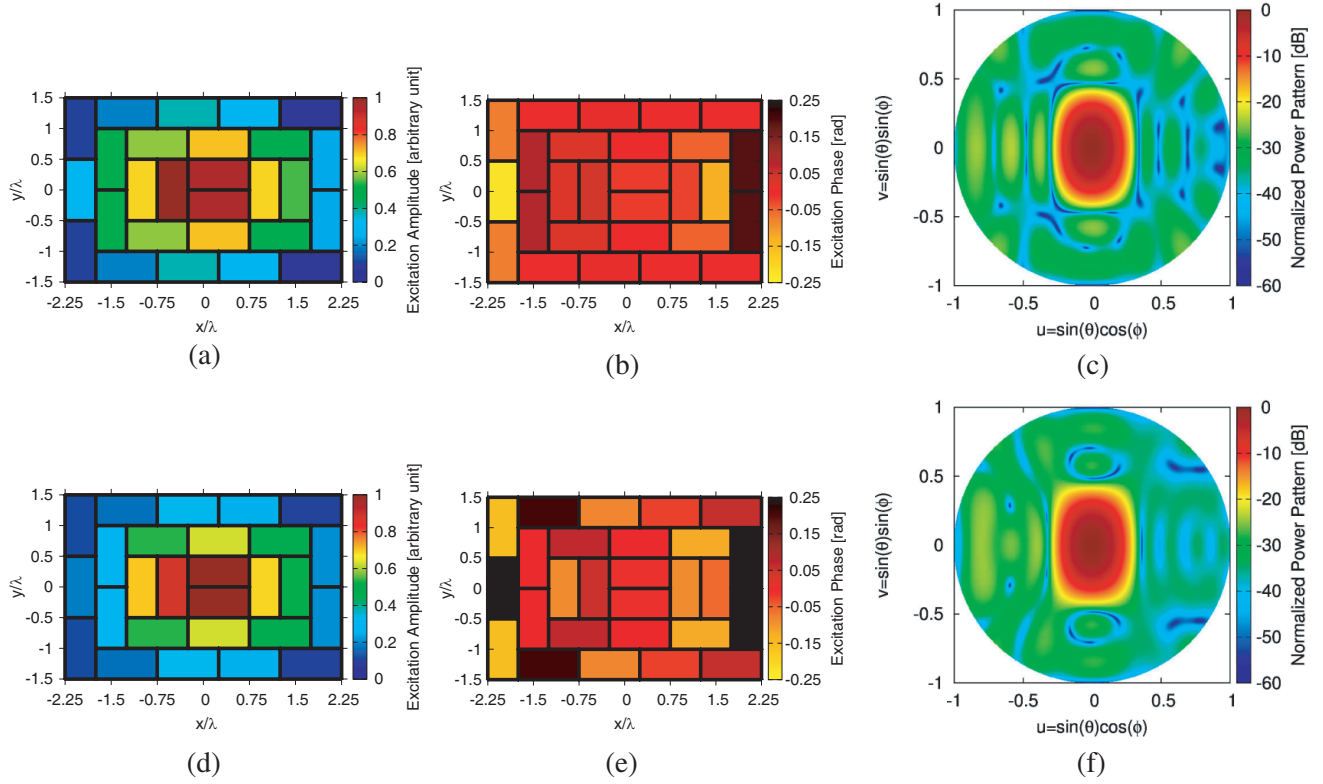
Figure 10. *Numerical Assessment (Medium Array, Asymmetric Mask; $d = 0.5\lambda$, $M \times N = 6 \times 9$ $N_{tot} = 54$, $T \simeq 8.2 \times 10^5$) — (a) (d) The tiles amplitudes excitations coefficients, (b) (e) the tiles phase excitations coefficients and (c) (f) the respective top-view power patterns of the EM-ETM, and the EM-OTM optimal solution (a) (b) (c), and the EM-ETM/CP solution (d) (e) (f).*
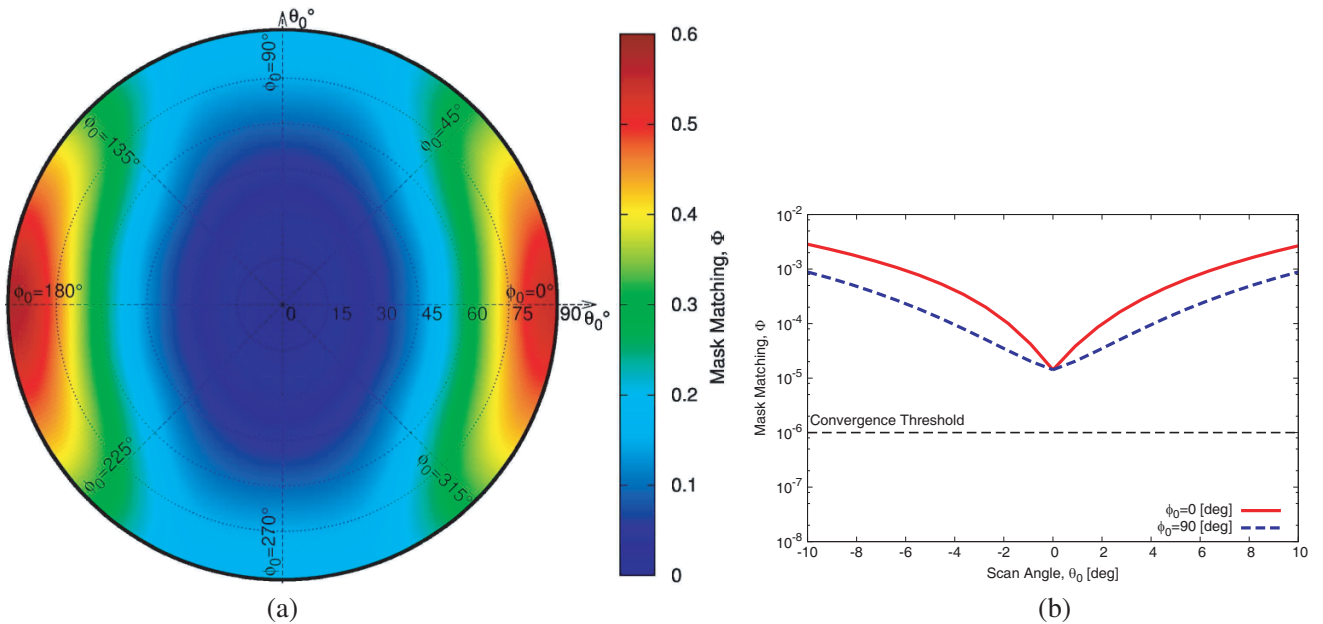

Figure 11. *Numerical Assessment (Medium Array, Asymmetric Mask; $d = 0.5\lambda$, $M \times N = 6 \times 9$ $N_{tot} = 54$, $T \simeq 8.2 \times 10^5$) — The mask matching map, evaluated when steering the beam of the EM-ETM/CP solution, within a scan cone.*

3.4. Reliability Assessment

In order to assess the reliability of the optimized solutions when considering real radiating elements, a set of test cases selected among the medium and large arrays previously designed have been simulated using
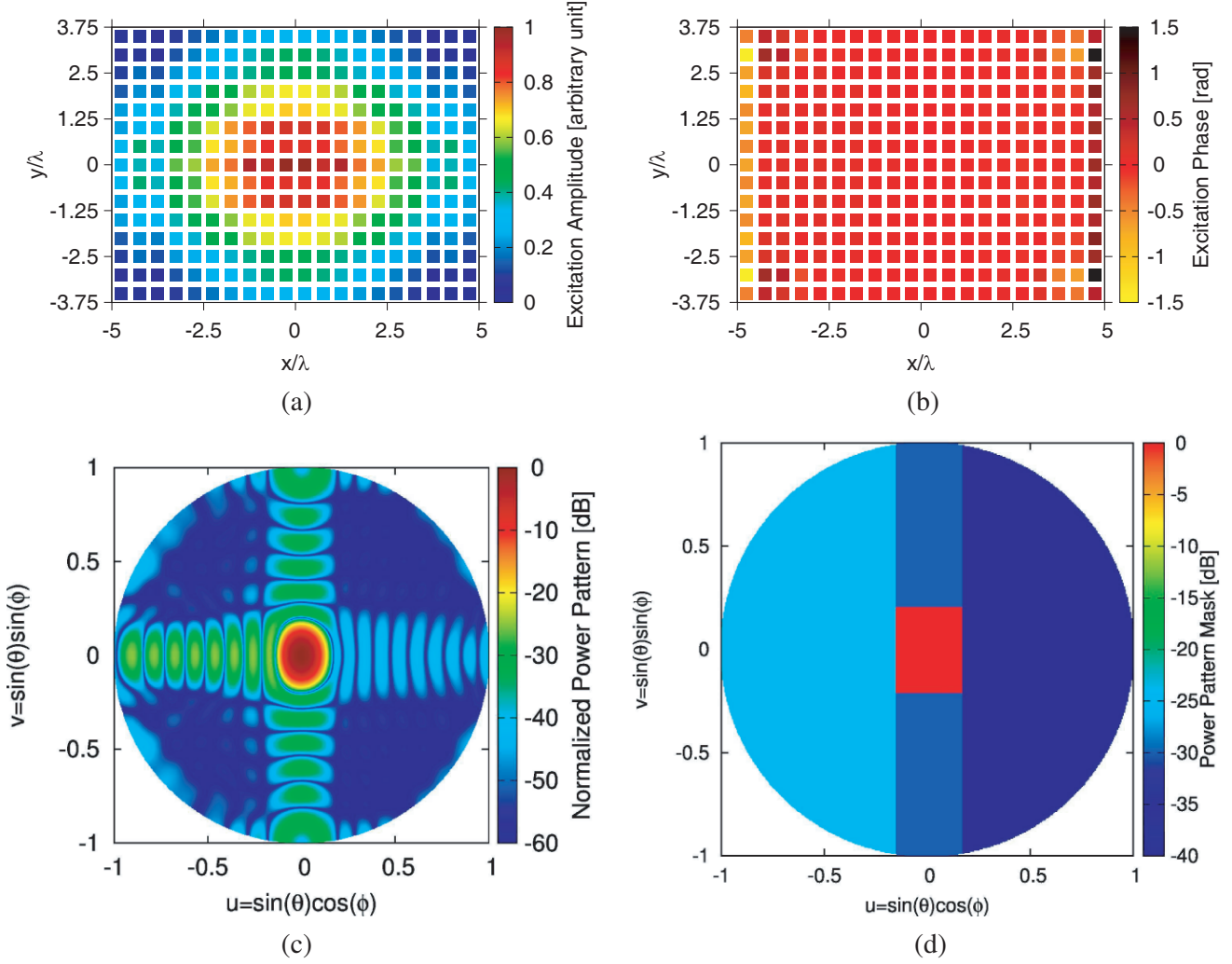

(a)

(b)

(c)

(d)

Figure 12. *Numerical Assessment (Large Array, Asymmetric Mask; $d = 0.5\lambda$, $M \times N = 15 \times 20$ $N_{tot} = 300$, $T \simeq 4.9 \times 10^{35}$) — The reference solution of the fully-populated array obtained through a CP optimization. (a) The amplitude coefficients, (b) the phase coefficients, and (c) the top-view power pattern, and (d) the synthesis mask.*

Table 5. Full-Wave Simulations — Measured radiation indexes (SLL, D, $HPBW_{az}$, and $HPBW_{el}$) and cost function Φ of the arrays simulated using the full-wave commercial software.

$M \times N$		SLL [dB]	D [dBi]	$HPBW_{az}$ [deg]	$HPBW_{el}$ [deg]	Φ -
6×9	$EM\text{-}ETM/CP$	-25.22	20.08	14.50	21.00	1.09×10^{-6}
	$EM\text{-}ETM$	-24.60	21.10	14.20	20.80	5.94×10^{-5}
15×20	$EM\text{-}OTM/CP$	-25.30	28.40	6.40	8.50	5.62×10^{-7}
	$EM\text{-}OTM$	-25.04	28.40	6.40	8.40	1.28×10^{-6}

(a)

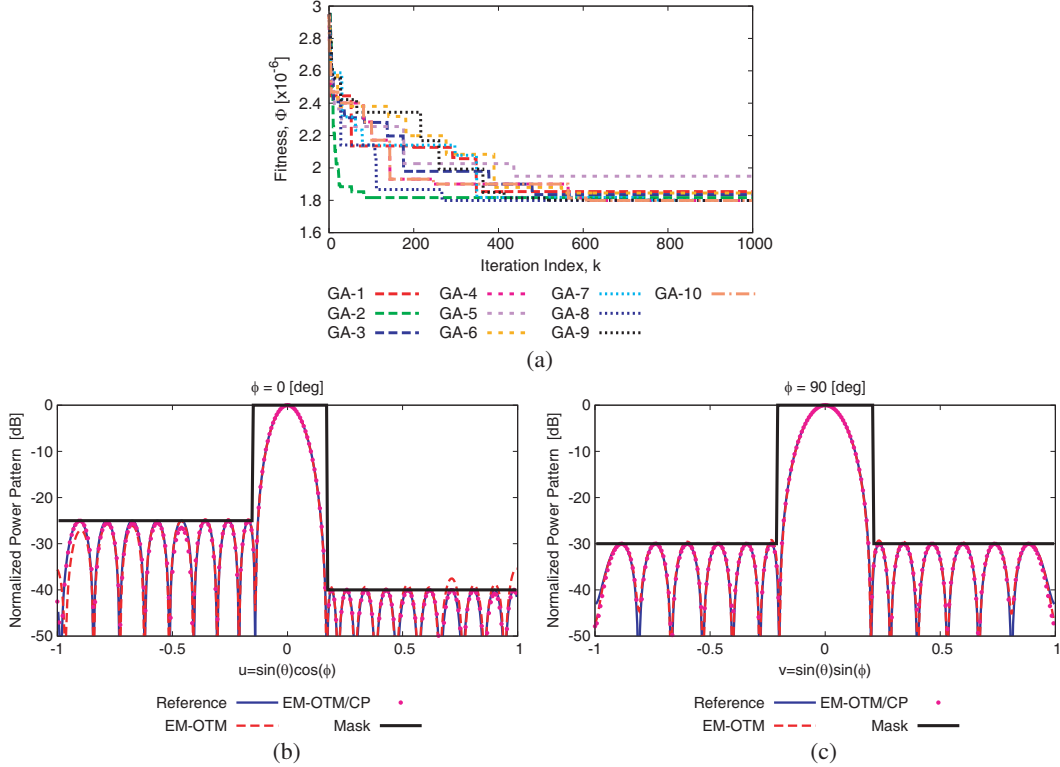(b)   (c)

Figure 13. *Numerical Assessment (Large Array, Asymmetric Mask; $d = 0.5\lambda$, $M \times N = 15 \times 20$ $N_{tot} = 300$, $T \simeq 4.9 \times 10^{35}$) — (a) The EM-OT simulation cost function evaluations for the 10 GA simulation runs. (b) (c) The power pattern cuts along the $u = u_0 = 0.0$ and $v = v_0 = 0.0$ plane of the EM-OTM optimal solutions and the EM-OTM/CP, as compared to the power mask.*
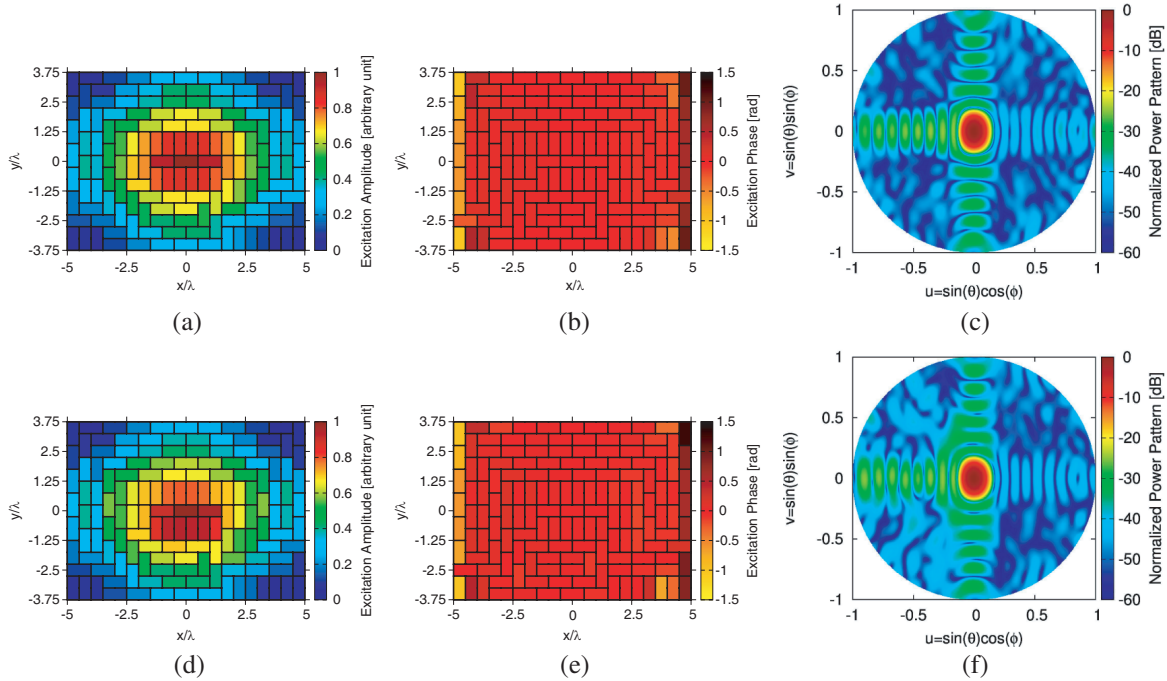

(a)   (b)   (c)

(d)   (e)   (f)

Figure 14. *Numerical Assessment (Large Array, Asymmetric Mask; $d = 0.5\lambda$, $M \times N = 15 \times 20$ $N_{tot} = 300$, $T \simeq 4.9 \times 10^{35}$) — (a) (d) The tiles amplitudes excitations coefficients, (b) (e) the tiles phase excitations coefficients and (c) (f) the respective top-view power patterns of the (a)–(c) EM-OTM optimal solution, and the (d)—(f) EM-OTM/CP solution.*
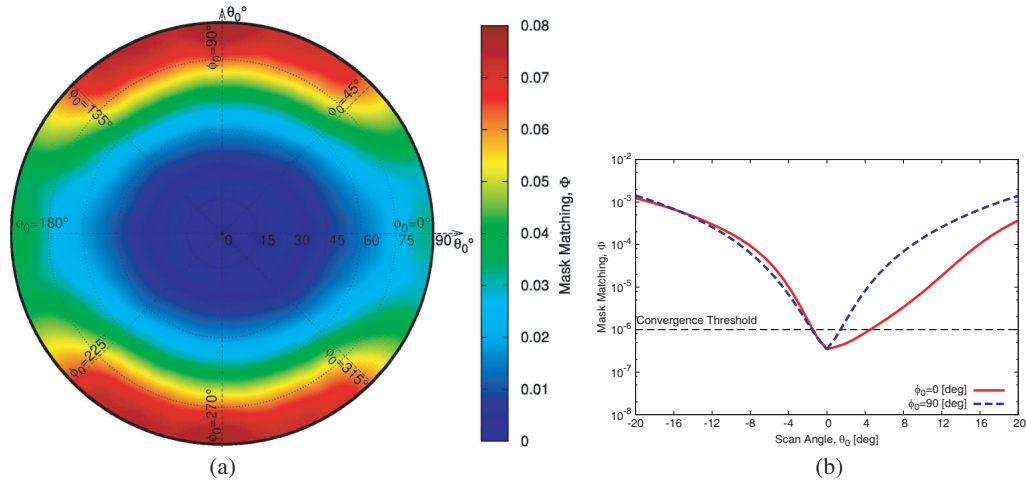
Figure 15. *Numerical Assessment (Large Array, Asymmetric Mask; $d = 0.5\lambda$, $M \times N = 15 \times 20$ $N_{tot} = 300$, $T \simeq 4.9 \times 10^{35}$) — The mask matching map, evaluated when steering the beam of the EM-OTM/CP solution, within a scan cone.*
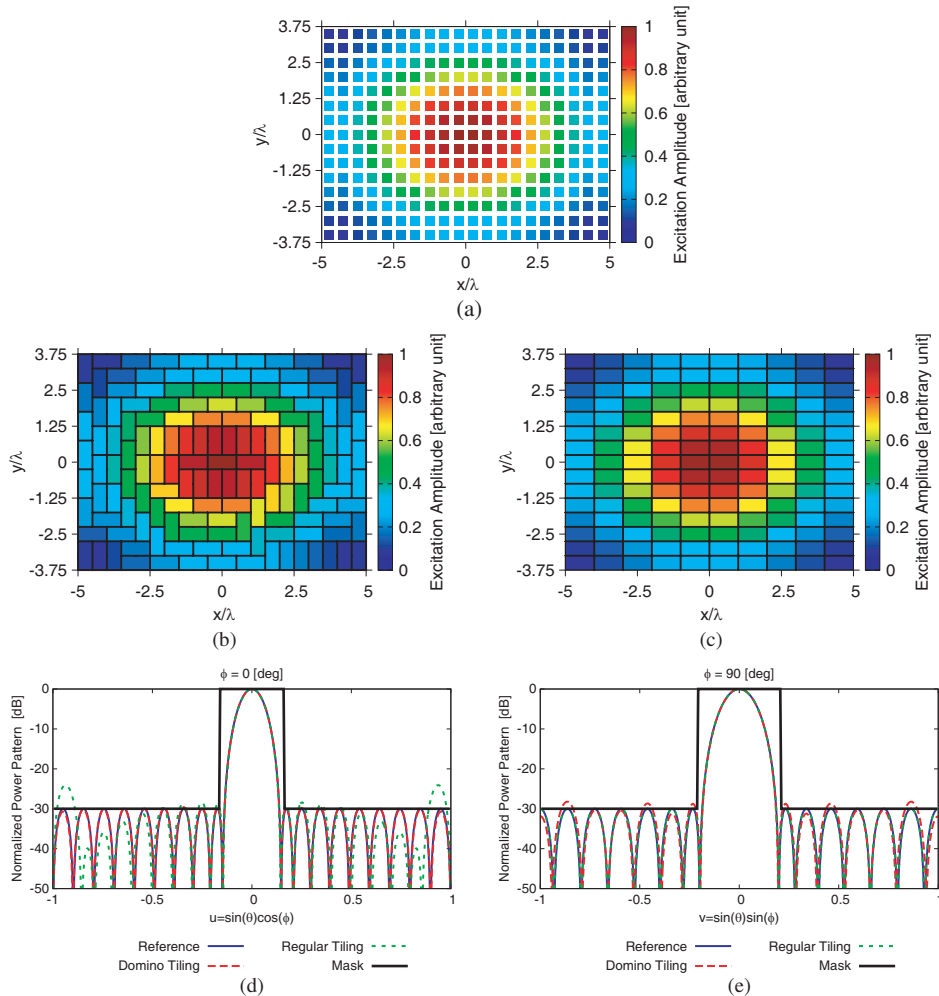

Figure 16. *Numerical Assessment (Large Array, Asymmetric Mask; $d = 0.5\lambda$, $M \times N = 15 \times 20$ $N_{tot} = 300$, $T \simeq 4.9 \times 10^{35}$) — (a) The Dolph-Chebyshev amplitude distribution (b) the EM-OTM optimal solutions, (c) a trivial regular domino tiling, and (d) (e) the power patterns along the main cuts as compared to the power mask.*
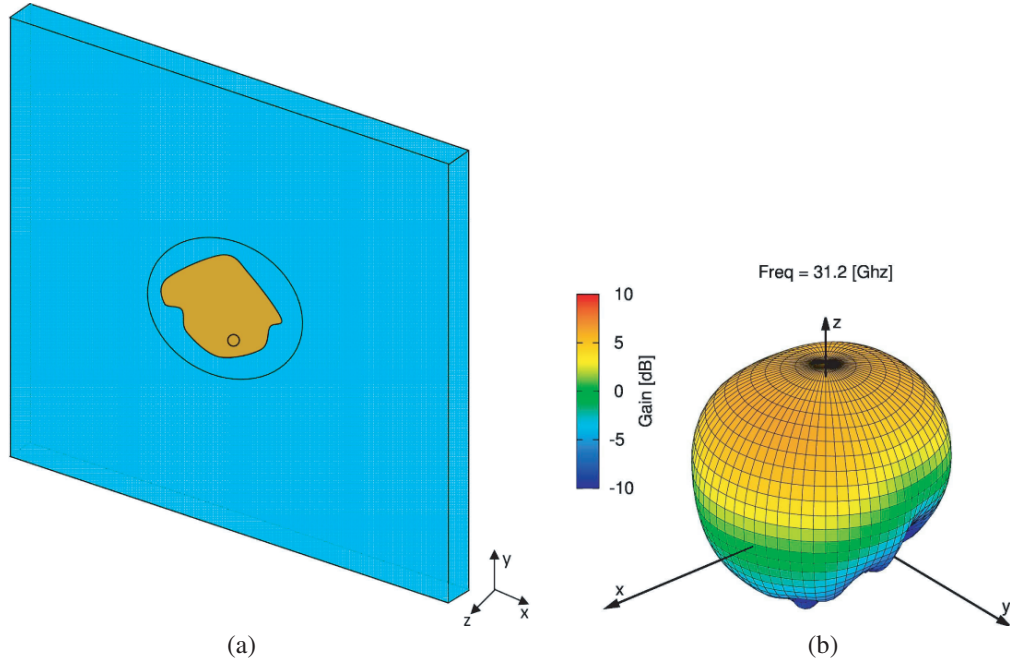
Figure 17. *Numerical Assessment* (*Full-Wave Simulations*) — (a) The model of the multi-layer patch antenna and (b) the cavity backed spline patch antenna considered for the full-wave simulations.
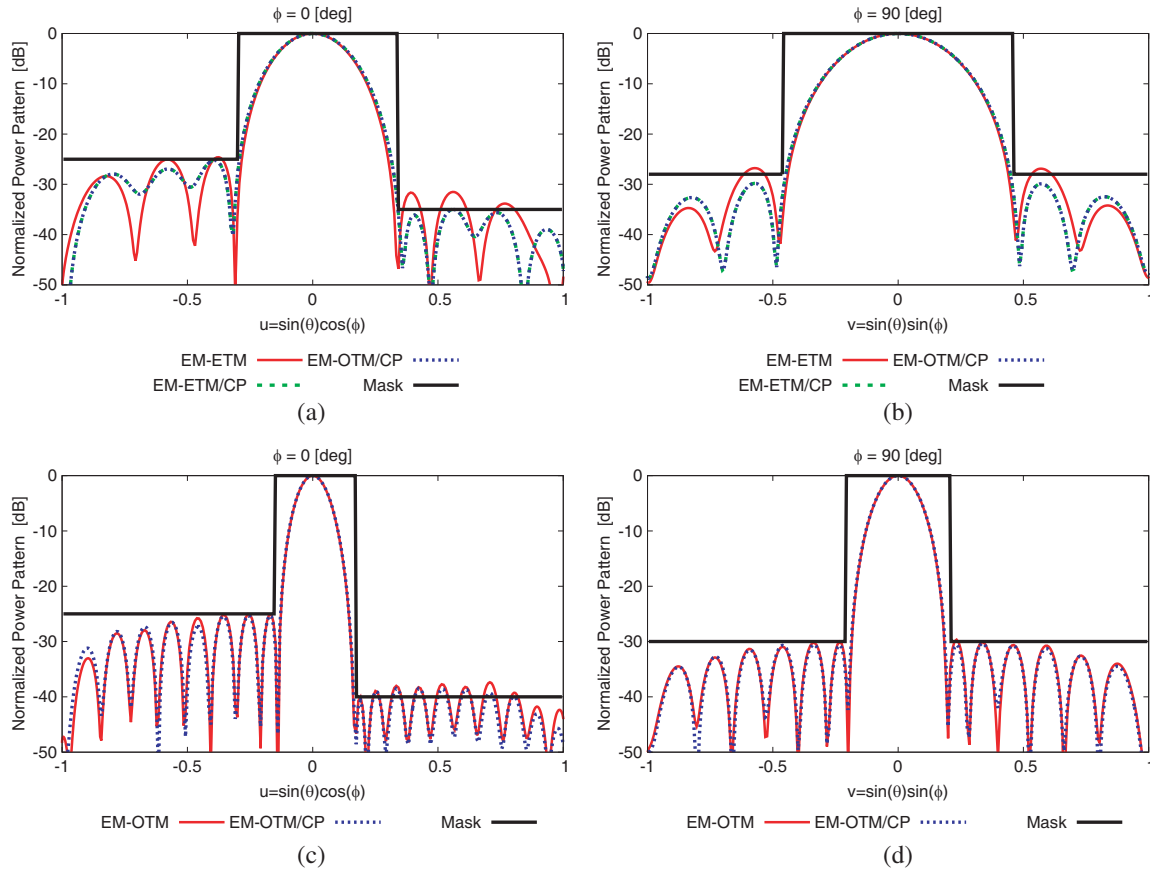

Figure 18. *Full-Wave Simulations* - The normalized power pattern cuts along (a) (c) the $u = u_0 = 0.0$ and (b) (d) $v = v_0 = 0.0$ planes of the *EM-OTM*, and the *EM-OTM/CP* methods for the $M \times N = 6 \times 9$ (a) (b) and $M \times N = 15 \times 20$ (c) (d) arrays as compared to the reference mask.

a commercial full-wave software. The cavity-backed spline-shaped patch (Fig. 17) has been considered. The power pattern cuts along the $\phi_0 = 0$ [deg] and $\phi_0 = 90$ [deg] planes of the simulated medium ($M \times N = 6 \times 9$) and large ($M \times N = 15 \times 20$) arrays are compared with the mask as reported in Fig. 18. As can be observed, the full-wave patterns of the proposed methods solutions (i.e., $ETM\text{-}CP$, $EM\text{-}ETM/CP$ and $EM\text{-}OTM/CP$) outperform the $EM\text{-}ETM$ solution pattern in terms of mask matching in all the considered cases (e.g., $\Phi^{EM\text{-}ETM/CP}|^{6\times9}_{Multi\text{-}Layer} = 6.91 \times 10^{-6}$ vs. $\Phi^{EM\text{-}ETM/CP}|^{6\times9}_{Multi\text{-}Layer} = 3.58 \times 10^{-5}$ and $\Phi^{EM\text{-}OTM/CP}|^{15\times20}_{Spline} = 5.62 \times 10^{-7}$ vs. $\Phi^{EM\text{-}ETM}|^{15\times20}_{Spline} = 1.28 \times 10^{-6}$, Table 5).

4. CONCLUSIONS

This work presents a novel class of optimization techniques for the design of rectangular tiled phased arrays when considering domino-like tiles and affording a pattern that minimizes the deviation from an user-defined upper-bound mask. According to the size of the array aperture, three different novel techniques have been proposed, namely the $ETM\text{-}CP$, $EM\text{-}ETM/CP$, and $EM\text{-}OTM/CP$, jointly optimizing the tiling configuration and the amplitude and/or phase excitation coefficients of the tiles modules, combining analytic and optimization-based domino tiling techniques with CP-based synthesis methods. A set of representative numerical results validate the proposed methods, for small, medium, and large array sizes, considering both symmetric and asymmetric masks. Moreover, the robustness of the optimized tiled array when steering the main beam within the visible range, as well as the reliability assessment when considering real radiating elements, through a full-wave simulations, has been analyzed. The numerical assessment leads to the following outcomes:

- the proposed exhaustive $ETM\text{-}CP$ approach has been effectively used for the optimization of very small arrays, but it turns out to be impractical for small/medium arrays due to the high computational burden introduced by the optimization of the tiles control points;
- even if a perfect matching cannot be always ensured (e.g., as shown by the design of medium sized arrays considering asymmetric masks) the reported results show that the proposed $EM\text{-}ETM/CP$ and $EM\text{-}OTM/CP$ methods allow to improve the matching with the mask-defined requirements with respect to the "bare" $EM\text{-}ETM$ and $EM\text{-}OTM$ optimizations.
- the reliability of the proposed methodologies has been assessed considering realistic patch antenna elements, positively compared with respect to the "bare" $EM\text{-}ETM$ and $EM\text{-}OTM$ solutions in terms of mask matching of the radiated pattern obtained using a commercial full-wave solver.

REFERENCES

1. Rocca, P., G. Oliveri, R. J. Mailloux, and A. Massa, "Unconventional phased array architectures and design Methodologies — A review," *Proc. IEEE*, Vol. 104, No. 3, 544–560, Mar. 2016.

2. Bucci, O. M., M. D'Urso, T. Isernia, P. Angeletti, and G. Toso, "Deterministic synthesis of uniform amplitude sparse arrays via new density taper techniques," *IEEE Trans. Antennas Propag.*, Vol. 58, No. 6, 1949–1958, Jun. 2010.

3. Haupt, R. L., "Adaptively thinned arrays," *IEEE Trans. Antennas Propag.*, Vol. 63, No. 4, 1626–1632, Apr. 2015.

4. Salucci, M., G. Gottardi, N. Anselmi, and G. Oliveri, "Planar thinned array design by hybrid analytical-stochastic optimization," *IET Microw. Antennas Propag.*, Vol. 11, No. 13, 1841–1845, Oct. 2017.

5. Oliveri, G., A. Gelmini, A. Polo, N. Anselmi, and A. Massa, "System-by-design multi-scale synthesis of task-oriented reflectarrays," *IEEE Trans. Antennas Propag.*, Vol. 68, No. 4, 2867–2882, Apr. 2020.

6. Salucci, M., A. Gelmini, G. Oliveri, N. Anselmi, and A. Massa, "Synthesis of shaped beam reflectarrays with constrained geometry by exploiting non-radiating surface currents," *IEEE Trans. Antennas Propag.*, Vol. 66, No. 11, 5805–5817, Nov. 2018.

7. Guan, D., Z. Qian, Y. Zhang, and J. Jin, "High-gain SIW cavity-backed array antenna with wideband and low sidelobe characteristics," *IEEE Antennas Wireless Propag. Lett.*, Vol. 14, 1774–1777, 2015.

8. Rocca, P., L. Manica, and A. Massa, "Synthesis of monopulse antennas through iterative contiguous partition method," *Electron. Lett.*, Vol. 43, No. 16, 854–856. 2007.

9. Manica, L., P. Rocca, A. Martini, and A. Massa, "An innovative approach based on a tree-searching algorithm for the optimal matching of independently optimum sum and difference excitations," *IEEE Trans. Antennas Propag.*, Vol. 56, No. 1, 58–66, Jan. 2008.

10. D' Urso, M., T. Isernia, and E. F. Meliado, "An effective hybrid approach for the optimal synthesis of monopulse antennas," *IEEE Trans. Antennas Propag.*, Vol. 55, No. 4, 1059–1066, 2007.

11. Rocca, P., M. H. Hannan, L. Poli, N. Anselmi, and A. Massa, "Optimal phase-matching strategy for beam scanning of sub-arrayed phased arrays," *IEEE Trans. Antennas Propag.*, Vol. 67, No. 2, 951–959, Feb. 2019.

12. Mailloux, R. J., S. G. Santarelli, and T. M. Roberts, "Wideband arrays using irregular (polyomino) shaped subarrays," *Electronics Lett.*, Vol. 42, No. 18, 1019–1020, Aug. 2006.

13. Mailloux, R. J., S. G. Santarelli, T. M. Roberts, and D. Lu, "Irregular polyomino-shaped subarrays for space-based active arrays," *Int. J. Antennas Propag.*, Vol. 2009, Article ID 956524, 2009.

14. Morabito, A. F., T. Isernia, M. G. Labate, M. Durso, and O. M. Bucci, "Direct radiating arrays for satellite communications via aperiodic tilings," *Progress In Electromagnetics Research*, Vol. 93, 107–124, 2009.

15. Yang, X., W. Xi, Y. Su, T. Zeng, T. Long, and T. K. Sarkar, "Optimization of subarray partition for large planar phased array radar based on weighted K-means clustering method," *IEEE Trans. Antennas Propag.*, Vol. 9, No. 8, 1460–1468, Dec. 2015.

16. Rocca, P., R. J. Mailloux, and G. Toso, "GA-based optimization of irregular sub-array layouts for wideband phased arrays design," *IEEE Antennas Wireless Propag. Lett.*, Vol. 14, 131–134, 2015.

17. Oppermann, M. and R. Rieger, "RF modules (Tx-Rx) with multifunctional MMICs," *2017 IMAPS Nordic Conference on Microelectronics Packaging (NordPac)*, 57–60, IEEE, Jun. 2017.

18. Lyon, R., A. Kinghorn, G. Morrison, A. Stonehouse, G. Byrne, and M. Dugan, "Active electronically scanned tiled array antenna," *IEEE International Symposium on Phased Array Systems and Technology*, 160–164, Oct. 2013.

19. Xiong, Z. Y., Z. H. Xu, S. W. Chen, and S. P. Xiao, "Subarray partition in array antenna based on the algorithm X," *IEEE Antennas Wireless Propag. Lett.*, Vol. 12, 906–909, 2013.

20. Anselmi, N., P. Rocca, and A. Massa, "Irregular phased array tiling by means of analytic schemata-driven optimization," *IEEE Trans. Antennas Propag.*, Vol. 65, No. 9, 4495–4510, Sep. 2017.

21. Diao, J., J. W. Kunzler, and K. F. Warnick, "Sidelobe level and aperture efficiency optimization for tiled aperiodic array antennas," *IEEE Trans. Antennas Propag.*, Vol. 65, No. 12, 7083–7090, Jan. 2017.

22. Ma, Y., S. Yang, Y. Chen, S. Qu, and J. Hu, "Pattern synthesis of 4-D irregular antenna arrays based on maximum-entropy model," *IEEE Trans. Antennas Propag.*, Vol. 67, No. 5, 3048–3057, May 2019.

23. Dong, W., Z.-H. Xu, X.-H. Liu, L.-S.-B. Wang, and S.-P. Xiao, "Modular subarrayed phased-array design by means of iterative convex relaxation optimization," *IEEE Antennas Wireless Propag. Lett.*, Vol. 18, No. 3, 447–451, Jan. 2019.

24. Rocca, P., N. Anselmi, A. Polo, and A. Massa, "Modular design of hexagonal phased arrays through diamond tiles," *IEEE Trans. Antennas Propag.*, Vol. 68, No. 5, 3598–3612, May 2020.

25. Rocca, P., N. Anselmi, A. Polo, and A. Massa, "Pareto-optimal domino-tiling of orthogonal polygon phased arrays," *IEEE Trans. Antennas Propag.*, Vol. 70. No. 5, 3329–3342, May 2022.

26. Avser, B., J. Pierro, and G. M. Rebeiz, "Random feeding networks for reducing the number of phase shifters in limited-scan arrays," *IEEE Trans. Antennas Propag.*, Vol. 64, No. 11, 4648–4658, Nov. 2016.

27. Rocca, P., N. Anselmi, A. Polo, and A. Massa, "An irregular two-sizes square tiling method for the design of isophoric phased arrays," *IEEE Trans. Antennas Propag.*, Vol. 68, No. 6, 4437–4449, Jun. 2020.

28. Conwey, J. H. and J. C. Lagarias, "Tiling with polyominoes and combinatorial group theory," *J. Combinatorial Theory, Series A*, Vol. 53, 183–208, 1990.

29. Klarner, D. A., "Packing a rectangle with congruent N-ominoes," *J. Combinatorial Theory*, Vol. 7, 107–115, 1969.

30. Brualdi, R. A. and T. H. Foregger, "Packing boxes with harmonic bricks," *J. Combinatorial Theory*, Vol. 17, 81–114, 1974.

31. Barnes, F. W., "Packing the maximum number of $m \times n$ tiles in a large $p \times q$ rectangle," *Discrete Math.*, Vol. 26, 93–100, 1979.

32. Kasteleyn, P., "The statistics of dimers on a lattice I. The number of dimer arrangements on a quadratic lattice," *Physica*, Vol. 27, 1209–1225, 1961.

33. Thurston, W. P., "Conway's tiling groups," *The American Mathematical Monthly*, Vol. 97, No. 8, 757–773, Oct. 1990.

34. Desreux, S. and E. Remila, "An optimal algorithm to generate tilings," *J. Discrete Alg.*, No. 4, 168–180, 2006.

35. Gottardi, G., L. Poli, P. Rocca, A. Montanari, A. Aprile, and A. Massa, "Optimal monopulse beamforming for side-looking airborne radars," *IEEE Antennas Wireless Propag. Lett.*, Vol. 16, 1221–1224, 2017.

36. Wachter, A. and L. Biegler, "On the implementation of an interior-point filter line-search algorithm for large-scale nonlinear programming," *Math. Program.*, Vol. 106, 25–57, Mar. 2006.

37. Rocca, P., M. Benedetti, M. Donelli, D. Franceschini, and A. Massa, "Evolutionary optimization as applied to inverse scattering problems," *Inv. Prob.*, Vol. 24, 1–41, 2009.